https://doi.org/10.1016/j.trc.2020.02.001

Mitigate the Range Anxiety: Siting Battery Charging Stations for Electric Vehicle Drivers

Min Xu[a]*, *Hai Yang*[b], *Shuaian Wang*[c]

[a] *Department of Industrial and Systems Engineering, The Hong Kong Polytechnic University, Hung Hom, Hong Kong*

[b] *Department of Civil and Environmental Engineering, The Hong Kong University of Science and Technology, Clear Water Bay, Kowloon, Hong Kong, China*

[c] *Department of Logistics and Maritime Studies, The Hong Kong Polytechnic University, Hung Hom, Hong Kong*

Abstract

This study addresses the location problem of electric vehicle charging stations considering drivers' range anxiety and path deviation. The problem is to determine the optimal locations of EV charging stations in a network under a limited budget that minimize the accumulated range anxiety of concerned travelers over the entire trips. A compact mixed-integer nonlinear programming model is first developed for the problem without resorting to the path and detailed charging pattern pre-generation. After examining the convexity of the model, we propose an efficient outer-approximation method to obtain the ε-optimal solution to the model. The model is then extended to incorporate the charging impedance, e.g., the charging time and cost. Numerical experiments in a 25-node benchmark network and a real-life Texas highway network demonstrate the efficacy of the proposed models and solution method and analyze the impact of the battery capacity, path deviation tolerance, budget and the subset of OD pairs on the optimal solution and the performance of the system.

Keywords: EV charging station location; range anxiety; compact formulation; outer-approximation algorithm; path deviation.

---

* Corresponding author

Tel: +852 2766 6593

Fax: +852 2362 5267

E-mail: xumincee@gmail.com; min.m.xu@polyu.edu.hk (M. Xu)

1. Introduction

Electric vehicles (EVs) are believed to be one of the most promising ways to reduce fossil-fuel dependency and greenhouse gas emissions. The social and environmental benefits, together with the high energy-efficiency against its gasoline counterpart attribute to the increasing popularity of EV among travelers (Bunsen et al., 2018). Despite the sizable merits, the high upfront purchase price, limited driving range as well as the long charging time hinder the adoption of EVs on a large scale (Egbue and Long, 2012; Sierzchula et al., 2014; Xu et al., 2017c). The fear of running out of electricity before reaching the destinations or EV charging stations, referred to as "range anxiety" in the literature, was found to be a major obstacle to customers' purchasing intentions (Egbue and Long, 2012; Franke et al., 2012). A EV charging station network with sufficient coverage should be developed to alleviate the range anxiety of EV users, especially for long-distance trips, e.g., inter-city trips, and in turn, promote the adoption of EVs.

The current EV charging technologies can be broadly classified into three modes based on their power levels: AC Level 1 with maximum power 1.92 kW, AC Level 2 with maximum power 19.2 kW, and DC Level 3 with minimum power larger than 19.2 kW (CCR, 2014; Morrow et al., 2008). Level 1 and 2 EV charging stations are known as normal/slow charging facilities due to the low charging powers delivered by them. Since an EV generally requires multiple hours to get replenished by a normal EV charging station, these stations are recommended for home and workplace charging activities. On the contrary, Level 3 charging facilities, known as DC fast EV charging stations, can deliver a high charging power, and thus are very suitable for the public usage along highways in the metro or inter-metro area (Smith and Castellano, 2015). Although it offers a high charging efficiency, a fast EV charging station generally incurs substantial cost associated with the procurement, installation, operation, and maintenance of the station. For example, the procurement and installation costs of a DC fast EV charging station are estimated to $10,000-$40,000 and $4,000-$51,000, respectively (CCR, 2014; Smith and Castellano, 2015). The huge investment for charging infrastructure deployment, especially the fast EV charging stations along highway for inter-city trips, necessitates careful planning in an intelligent and optimized manner.

1.1 Literature review

Motivated by the above facts, many studies have been conducted for the optimal deployment of fast EV charging stations or refuelling infrastructures for EVs or other alternative-fuel vehicles (Arslan and Karaşan, 2016; Chen et al., 2016; Ghamami et al., 2016; He et al., 2013; He et al., 2015; He et at., 2018; 2020; Kim and Kuby, 2012; Kuby and Lim, 2005; Lee and Han, 2017; Li et al., 2016; Liu and Wang, 2017; Mak et al., 2013; Nie and Ghamami, 2013; Sathaye and Kelley, 2013; Wang et al., 2019; Wang and Wang, 2010; Yıldız et al., 2016; Yıldız et al., 2019; Zhang et al., 2020). Since EV charging stations are often visited en route, the charging demand should be modeled as path flows between origin-destination (OD) pairs on a network. For example, Hodgson (1990) proposed a flow-capturing location model (FCLM) to optimize the facility locations by capturing the traffic flows as much as possible. The FCLM was later extended by Kuby and Lim (2005) by considering multiple charging activities en route during a single trip in a flow refueling location model (FRLM). For the sake of model building, the concept of a feasible combination of refueling stations (also referred to as a charging pattern) that enables a successful journey was introduced. Kim and Kuby (2012) further extended the FRLM and developed a deviation-flow refueling location model (DFRLM) to take into account the travelers' deviation behavior from their intended shortest paths for charging. Both an illustrative example and the numerical experiments have demonstrated the necessity of allowing deviations in modeling flow refueling. The competency to incorporate multiple charging activities during a trip attracted many follow-up studies based on FRLM and RFRLM (Capar et al., 2013; Chung and Kwon, 2015; Huang et al., 2015; Kuby and Lim, 2007). The cumbersome pre-generation of feasible combinations of EV charging stations and deviation paths between OD pairs, however, limits the application of FRLM and RFRLM in large-scale networks (MirHassani and Ebrazi, 2012; Yıldız et al., 2016). A compact optimization model without the pre-generation of charging combinations and deviation paths is therefore highly anticipated.

In light of the frequent discussions of this psychological phenomenon, many studies sought an empirically based understanding of the range anxiety of EV drivers (Rauh et al., 2015). For example, Valentine-Urbschat and Bernhart (2009) found that range anxiety would negatively affect the drivers as soon as the battery charge falls below 50% of its capacity. Xu et al. (2017b) identified from probe EV data that the state of charge (SOC) of the battery affects the range anxiety in a nonlinear way. Graham-Rowe et al. (2012) found from a survey that the range anxiety of EV users was amplified when they observed the decreasing of battery charge while driving. Yang et al. (2016) and Xu et al. (2017a; 2017b) examined the effects of range anxiety on the charging and route choice behavior of EV users. Neubauer and Wood (2014) found that the effects of range anxiety on EVs' utility can be significant, but can be reduced by charging infrastructure. They employed the minimum range margin, also termed as the comfortable range threshold by Franke et al. (2012), as a proxy for range anxiety. Similarly, Yuan et al. (2018) found from a survey that recharge accessibility is a significant contributing factor for the range anxiety of EV drivers. Nilsson (2011) identified several approaches to mitigate range anxiety including an extensive deployment of fast EV charging stations that minimizes the occurrence of SOC falling below the comfortable range threshold of EV users. Dong et al. (2014) emphasized the significance of relieving travelers' range anxiety by optimizing the EV charging station deployment.

Though commonly acknowledged as a major obstacle for EV adoption, range anxiety was not adequately addressed in the context of EV charging station deployment (Guo et al., 2018; Yang et al., 2017). Most of the previous studies for station location problem, e.g., RFLM and DRFLM, merely maximized the covered or refueled flow demand without considering the experienced range anxiety of the travelers. The example of a simple path in Figure 1 intuitively illustrates the difference between the optimal EV charging station deployment suggested by the conventional FRLM or RFRLM and a model that minimizes the experienced range anxiety of the EV drivers. The value beside each link represents its electricity consumption expressed in percentage of battery capacity. We assume that the EV departs from the origin with a fully charged battery, and at most one station can be built due to a limited budget. The comfortable range threshold is 30%. It can be seen that either node B or node C will be selected by RFLM or DRFLM as the optimal EV charging station location, while only node C is deemed as an optimal location because by charging the EV at location C, the SOC of the EV during the entire trip will remain no less than 30%, and thus travelers are free from range anxiety. Since both location B and C can ensure a successful journey, the RFLM or DRFLM that merely maximizes the refueled flow cannot capture the differences between the two candidate locations. This example motivates us to pay special attention to the range anxiety of travelers when determining the deployment of EV charging stations.

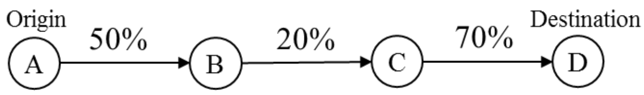

Figure 1. An illustrative example

Among the most related studies, Yang et al. (2017) characterized the effect of range anxiety and loss anxiety, i.e., the willingness to not swap or charge a battery because the remaining energy is still fairly high, on the customers' satisfaction in an EV service infrastructure network design problem under deterministic and fuzzy scenarios. They maximized the total profit by covering the satisfaction-constrained path flow volume. A hybrid algorithm combining the tabu search and the greedy randomized adaptive search procedure was developed to solve the problem. Guo et al. (2018) incorporated a flow decaying function with respect to range anxiety into the DRFLM. They developed a hybrid heuristic combining a modified k-shortest path algorithm, an iterative greedy heuristic, and an adaptive large-neighborhood search for the considered problem. Note that the above two studies interpreted the range anxiety as the maximal impendence incurred only at the point of charging, which actually corresponds to the worst-case scenario; whereas in reality, drivers will feel uncomfortable once the remaining electricity of their EVs falls below the comfortable range threshold. A station location model considering the entire profile of range anxiety experienced by EV drivers during the trip is expected.

1.2 Objective and contributions

To bridge the aforementioned gaps, this study investigates the deployment of fast EV charging stations problem to support inter-city travel considering drivers' range anxiety and path deviation, referred to as DCSP thereafter. We assume that the EVs have a limited driving range, and drivers are associated with a nonlinear range anxiety profile determined by the remaining electricity of their EVs, and they may take a deviation path other than the shortest path between an origin-destination (OD) pair for refueling. Since we consider inter-city highway travel, there could be multiple charging activities en route during a single trip. The objective of this study is to determine the optimal locations of EV charging stations that minimize the accumulated range anxiety of concerned travelers over the entire trips under a limit budget. To achieve this objective, we will first formulate a compact mixed-integer programming model by explicitly describing the charging logic and detour behavior, which favorably circumvents the computationally extensive path and combination pre-generation suffered by traditional FRLM/DFRLM. Due to the nonlinearity of range anxiety profile, the resultant nonlinear model was not readily solvable by state-of-art solvers. We thus propose an efficient outer-approximation method to obtain the ε-optimal solution to the problem. Here the ε-optimal solution refers to the solution that the error of its objective function value to the optimal objective function value is within an exogenously pre-specified maximum tolerance ε. To the best of our knowledge, so far no studies have ever developed a compact model in consideration of path deviation, and more importantly, incorporated the profile of range anxiety of EV drivers in the decision-making of EV charging station location. The aforementioned literature review validates the novelty of this study.

The remainder of this study is organized as follows. Assumptions, notations and problem statement are elaborated in Section 2. A compact mixed-integer nonlinear programming model for DCSP is formulated in Section 3. Section 4 linearizes the range anxiety profile by means of outer-approximation method, and the resultant mixed-integer linear programming (MILP) model can be readily solved by available solvers to obtain the ε-optimal solution. The extended model that incorporates the charging impedance is presented in Section 5. The efficiency of the proposed model and algorithm is demonstrated by the numerical experiments in a 25-node network and the real-world Texas highway network in Section 6. Section 7 presents conclusions and future research.

2. Assumptions, Notations and Problem Statement

We define the DCSP over a high-way network $\mathcal{G} = (\mathcal{N}, \mathcal{A})$ where $\mathcal{N}$ is the node set and $\mathcal{A}$ is the link set. Each link $(i, j) \in \mathcal{A}$, $i, j \in \mathcal{N}$ is associated with length l_{ij} and electricity consumption d_{ij}. All OD pairs are grouped into a set denoted by $\mathcal{W}$. The origin and destination node of a particular OD pair $w \in \mathcal{W}$ is represented by $r(w)$ and $s(w)$, respectively. Let f^w denote the flow volume of an OD pair $w \in \mathcal{W}$, which is assumed to be known a priori. Without loss of generality, we assume that EV charging stations have to be located in nodes of a transportation network among candidate locations in a set denoted by $\mathcal{I} \subseteq \mathcal{N}$. The construction of an EV charging station at location $i \in \mathcal{I}$ will incur a cost denoted by c_i. The total budget for EV charging station construction is represented by B. The battery capacity of EV measured by kWh is defined as the maximum electricity in battery per a full battery charge is denoted by E. The EVs are assumed to depart/arrive with initial/remaining electricity no larger/smaller than a known pre-specified threshold denoted by E_O / E_D. For simplicity, we assume that EVs can be fully replenished per charge at an EV charging station, and the EV charging stations to be established are uncapacitated.

Regarding travelers' route choice behavior, we assume that drivers would like to take a deviation path other than the shortest path for refueling, as long as the detour distance is within a pre-specified tolerance. Note that the value of deviation tolerance can be obtained by stated-preference-survey. Given the layout of EV charging stations, drivers are free to travel on any path (e.g., the path with the minimal detour distance) as long as the detour distance is within their tolerance. Let L^w be the length of the shortest path for an OD pair w, and η^w is a pre-specified tolerance for detour distance. The assumption means that the length of a feasible path for travelers of OD pair w should not exceed $L^w + \eta^w$. Note that depending on the travel distance of an OD pair, an EV may require multiple charges along a trip to ensure smooth traveling as assumed in the conventional FRLM and DFRLM. Drivers may experience range anxiety during the trips depending on the real-time SOC of their EVs. All the notations used throughout this study are provided in Appendix for readability. The objective of DCSP in this study is to deploy EV charging stations in the network so that (i) the traffic flow between each OD pair travels on a range-feasible path no longer than $L^w + \eta^w$ if any; (ii) the total construction cost is within the budget B; and (iii) the experienced accumulated range anxiety of the drivers during the entire trips is minimized.

2.1 Charging logic

The key to compact model building without resorting to path and charging combination generation is to formulate the charging logic directly in the model. Wang and Lin (2009) have illustrated and formally established the charging logic along a single path in their formulation. We extended their study by formulating the charging logic in a general network. To this end, we define two kinds of binary decision variables: a location variable y_i, $\forall i \in \mathcal{I}$ denoting whether a station will be built at location i, and a link variable x_{ij}^w, $\forall (i, j) \in \mathcal{A}$, $w \in \mathcal{W}$ denoting whether the flow of OD pair w will traverse link (i, j); as well as an auxiliary continuous variable e_i^w, $\forall i \in \mathcal{N}$, $w \in \mathcal{W}$ denoting the remaining electricity in battery rightly after traversing node i. The value of e_i^w for the traversed nodes along a path will follow a diminishing trend, indicating that the SOC of battery keeps decreasing along the trip. If, however, an EV charging station has been built in node i, the battery can be fully replenished at the EV charging station located in node i, and e_i^w will accordingly be reset to E.

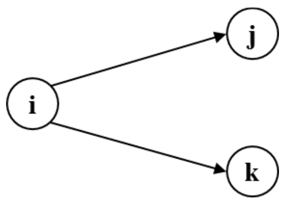

Figure 2. An illustrative sub-network consisting of two links

To illustrate the formulation of charging logic in a general network, we use a typical part of a network consisting of two links (i, j) and (i,k) that share the same head node i as shown in Figure 2. It is straightforward that we shall have the following constraint to ensure the feasibility of a link, e.g., link (i, j) :

$$e_i^w \geq d_{ij} x_{ij}^w \tag{1}$$

For the EVs between OD pair w, given the value of $e_i^w \in [0, E]$ at node i, our next purpose is to express e_j^w at its adjacent node j such that $(i, j) \in \mathcal{A}$. Therefore we need to consider the following cases:

If node j is chosen as an EV charging station location and the flow traverses link (i, j), i.e., $y_j = 1$ and $x_{ij}^w = 1$, we have

$$e_j^w = E \qquad (2)^1$$

If node j is chosen as an EV charging station location and the flow does not traverse link (i, j), i.e., $y_j = 1$ and $x_{ij}^w = 0$ (e.g., the flow may traverse another link (i,k) originating from node i), we have a null constraint:

$$0 \leq e_j^w \leq E \tag{3}$$

If node j is not chosen as an EV charging station location but the flow traverses link (i, j), i.e., $y_j = 0$ and $x_{ij}^w = 1$, we have

$$e_j^w = e_i^w - d_{ij} \tag{4}$$

If node j is not chosen as an EV charging station location and the flow does not traverse link (i, j), i.e., $y_j = 0$ and $x_{ij}^w = 0$, again we have a null constraint:

$$0 \leq e_j^w \leq E \tag{5}$$

We proceed to consolidate the above constraints by linking the decision variables with Eqs. (2)-(5). Since Eqs. (3) and (5) are null constraints, our main objective is to express Eqs. (2) and

[1] The implicit assumption herein is that the EV will always charge at traversed stations. This assumption is not restrictive because our objective is to minimize the accumulated range anxiety of the drivers during the entire trips and thus the optimality of a solution will by nature assure that $e_j^w = E$ if $y_j = 1$ and $x_{ij}^w = 1$.

(4). Specifically, to express Eq. (2) without violating Eqs. (3)-(5) by linking the location variable y_j with e_j^w, we have

$$Ey_j \le e_j^w \le E \tag{6}$$

We continue to express Eq. (4) without violating Eqs. (2), (3) and (5). To protect Eq. (2), a component Ey_j should be used to lift the bound on the right-hand side of Eq. (4), i.e.,

$$e_j^w \le e_i^w - d_{ij} + Ey_j \tag{7}$$

As for Eqs. (3) and (5), since under both cases it holds that $x_{ij}^w = 0$, we cannot guarantee $e_i^w \ge d_{ij}$ from Constraint (1). Hence we need another component $d_{ij}(1-x_{ij}^w)$ to ensure the positiveness of $e_i^w - d_{ij}$ in the original Eq. (4). Besides, Eq. (5) entails an additional component $E(1-x_{ij}^w)$. In summary, we have

$$e_j^w \le e_i^w - d_{ij} + Ey_j + d_{ij}(1-x_{ij}^w) + E(1-x_{ij}^w) \tag{8}$$

which is consolidated to be

$$e_j^w \le e_i^w - d_{ij}x_{ij}^w + E(1-x_{ij}^w + y_j) \tag{9}$$

The above procedure has consolidated the original Eqs. (2)-(5) and the correspondent conditions into Constraints (6) and (9).

2.2 Driving range anxiety

Although it is widely acknowledged that the deployment of EV charging stations affects drivers' range anxiety, no studies were dedicated to the analytical relationship specification or calibration between the EV charging station deployment and EV drivers' range anxiety. Fortunately, the limited studies for range anxiety reviewed in Subsection 1.1 gave us the following insights:

1. Range anxiety is largely affected by the remaining electricity of battery (Xu et al., 2017b; Yang et al., 2016);
2. There has been a comfortable range threshold that frees EV drivers from range anxiety (Franke et al., 2012; Guo et al., 2018; Yuan et al., 2018);
3. Range anxiety would increase as the SOC approaches zero, and the rate of variation also increases with the decrease of SOC (Xu et al., 2017b).

Based on the above findings, we assume that the range anxiety of an EV driver will convexly decrease from a maximal value $R_{\max}$ with the increase of remaining electricity in the battery until the amount of remaining electricity reaches a comfortable range threshold denoted by E_{comf}, and after that the range anxiety will remain at 0 before the SOC achieves its maximal value E. This assumption is also consistent with the concave shape of customers' satisfaction function (e.g., inverse range anxiety) against service quality (e.g., SOC) in the field of management and marketing (Anderson and Sullivan, 1993; Chen and Chen, 2014; Grigoroudis and Siskos, 2009). For ease of presentation, SOC in this study represents the absolute level of charge of an electric battery unless stated otherwise. Figure 3 illustrates the variation of drivers' range anxiety against the SOC (i.e., the remaining electricity in the battery).

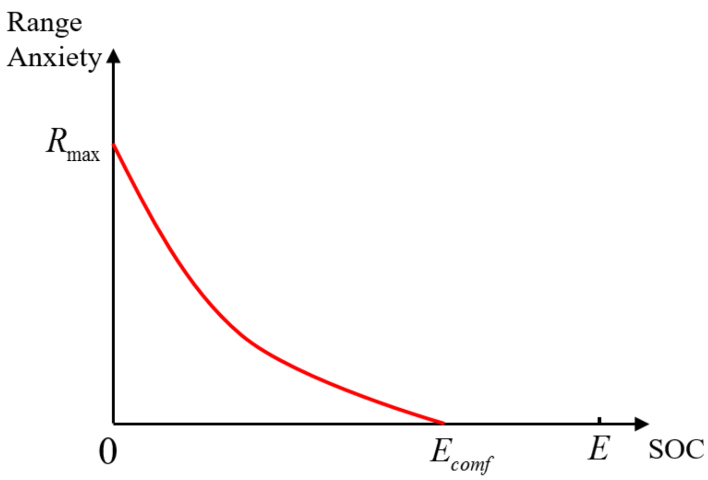

Figure 3. The variation of drivers' range anxiety against the SOC

According to the studies for battery discharging behavior of EVs, the SOC of a battery will decrease almost linearly with the travel time under a constant driving speed (Pelletier et al., 2017; Xu and Meng, 2019). After the SOC falls below E_{comf}, e.g., at time t^*, the range anxiety, accordingly, will start increasing convexly along the trip until the EV is fully replenished at an EV charging station and the range anxiety returns to 0. We assume for simplicity that the profile of SOC and the range anxiety of drivers follow a linear and a convex function denoted by $S(t)$ and $R(t)$ respectively under a constant traveling speed. Figure 4 shows the profile of the remaining electricity and range anxiety over one cycle, whereas the iterative procedure over an entire trip is illustrated in Figure 5.

For the sake of model building, we define the sub-path from the origin to the first charging station, the sub-paths between two adjacent EV charging stations, and the sub-path from the last EV charging station to the destination as path segments. Let r denote the final SOC at the end node of a path segment. The accumulated range anxiety along a path segment, i.e., the shaded area in Figure 5, can thus be calculated by

$$\bar{R}(r) = \int_0^{S^{-1}(r)} R(t)dt \tag{10}$$

where $S^{-1}(\bullet)$ is the inverse function of $S(\bullet)$. Exactly speaking, the accumulated range anxiety of the first path segment is also dependent on the SOC at departure, and should be calculated by $\int_{S^{-1}(E_o)}^{S^{-1}(r)} R(t)dt$. However, according to the range anxiety profile in Figure 4, the accumulated range anxiety expressed by $\int_{S^{-1}(E_o)}^{S^{-1}(r)} R(t)dt$ will reduce to $\int_0^{S^{-1}(r)} R(t)dt$ if the initial SOC is no smaller than the comfortable range threshold, i.e., $E_O \geq E_{comf}$.

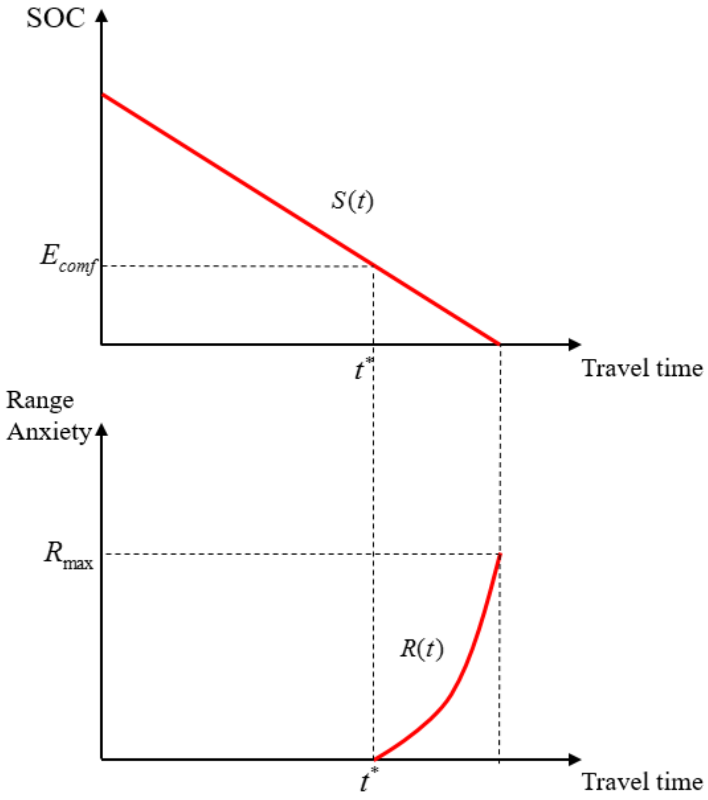

Figure 4. The profile of SOC and drivers' range anxiety over one cycle

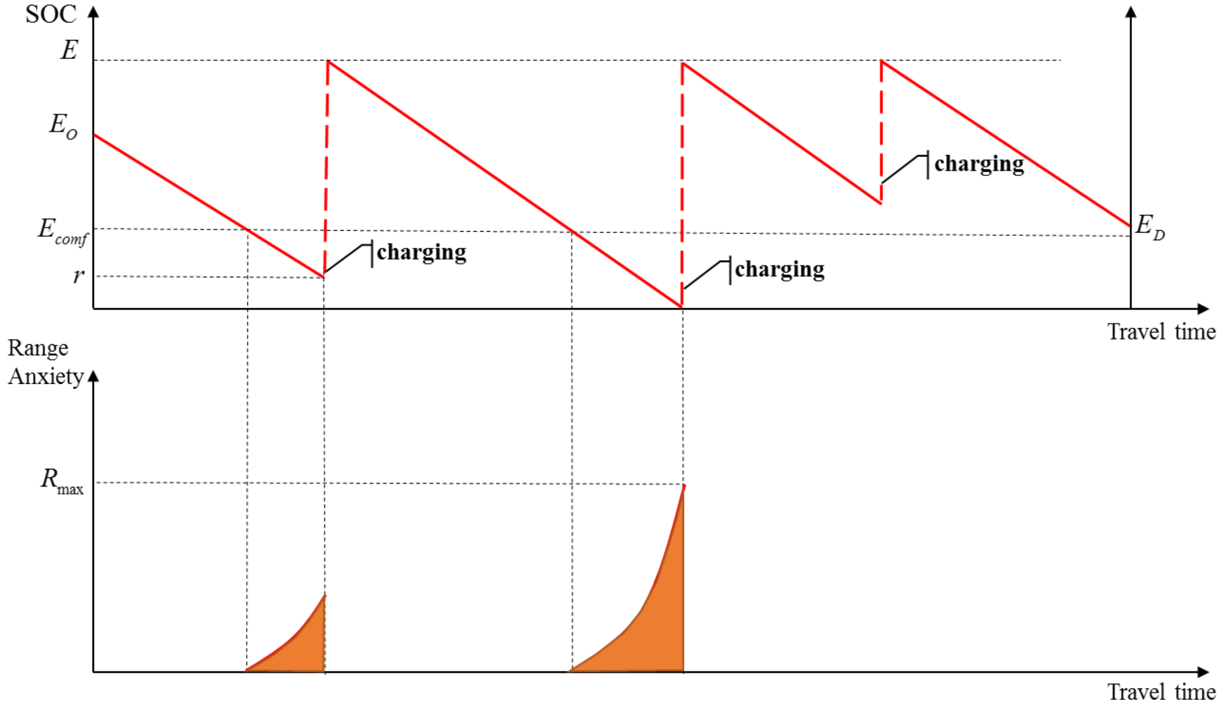

Figure 5. The profile of SOC and drivers' range anxiety over a trip

Since each path segment is uniquely characterized by its end node, which is either a traversed EV charging station or the destination, we can express the accumulated range anxiety over an entire trip as the sum of accumulated range anxiety function of each path segments with respect to the SOC upon arriving an EV charging station or a destination. Specifically, let r_j^w, $\forall j \in \mathcal{I} \cup \{s(w)\}$ denote the SOC upon the EVs of OD pair w arriving an EV charging station $j \in \mathcal{I}$ or the destination $s(w)$; it follows that

$$r_j^w \le e_i^w - d_{ij} x_{ij}^w + E(1 - x_{ij}^w), \quad \forall (i,j) \in \mathcal{A}, j \in \mathcal{I} \cup \{s(w)\}, w \in \mathcal{W} \tag{11}$$

The total accumulated range anxiety of the EV drivers between all OD pairs can thus be calculated by

$$TARA = \sum_{w \in \mathcal{W}} f^w \left[\sum_{j \in \mathcal{I}} \bar{R}(r_j^w) y_j + \bar{R}(r_{s(w)}^w) \right] \tag{12}$$

3. Optimization Model Building

3.1 Model formulation

To accommodate the case that the flows of an OD pair cannot be refueled due to the limited driving range or budget, we create a zero-distanced auxiliary link connecting the origin and destination of an OD pair w, i.e., link ($r(w)$, $s(w)$), upon the original network. To ensure range feasibility of this auxiliary link, the electricity consumption $d_{r(w)s(w)}$ is set to be zero if $E_O \geq E_D$, and $(E_O - E_D)$ otherwise. With above the notations, the DCSP can be formulated upon the network with an updated link set $\mathcal{A} \leftarrow \mathcal{A} \bigcup \{(r(w), s(w))\}_{w \in \mathcal{W}}$ by the following model:

[DCSP]

$$\min_{\mathbf{x},\mathbf{y},\mathbf{e},\mathbf{r}} \quad Obj(\mathbf{x},\mathbf{y},\mathbf{e},\mathbf{r}) = TARA + M \sum_{w \in \mathcal{W}} f^{w} x^{w}_{r(w)s(w)} \tag{13}$$

subject to

$$\sum_{\{j|(i,j)\in\mathcal{A}\}} x^w_{ij} - \sum_{\{j|(j,i)\in\mathcal{A}\}} x^w_{ji} = \begin{cases} 1, & i = r(w) \\ -1, & i = s(w) \\ 0, & i \in \mathcal{I} \end{cases} \quad \forall w \in \mathcal{W} \tag{14}$$

$$\sum_{i \in \mathcal{I}} c_i y_i \leq B \tag{15}$$

$$e^w_j \leq e^w_i - d_{ij} x^w_{ij} + E(1 - x^w_{ij} + y_j), \quad \forall j \in \mathcal{I}, (i,j) \in \mathcal{A}, w \in \mathcal{W} \tag{16}$$

$$E y_j \leq e^w_j \leq E, \quad \forall j \in \mathcal{I}, w \in \mathcal{W} \tag{17}$$

$$d_{ij} x^w_{ij} \leq e^w_i, \quad \forall (i,j) \in \mathcal{A}, w \in \mathcal{W} \tag{18}$$

$$e^w_j \leq e^w_i - d_{ij} x^w_{ij} + E(1 - x^w_{ij}), \quad \forall j \in \mathcal{N} \setminus \mathcal{I}, (i,j) \in \mathcal{A}, w \in \mathcal{W} \tag{19}$$

$$0 \leq e^w_j \leq E, \quad \forall j \in \mathcal{N} \setminus \mathcal{I}, w \in \mathcal{W} \tag{20}$$

$$r^w_j \leq e^w_i - d_{ij} x^w_{ij} + E(1 - x^w_{ij}), \quad \forall j \in \mathcal{I} \bigcup \{r(w)\}, (i,j) \in \mathcal{A}, w \in \mathcal{W} \tag{21}$$

$$0 \leq r^w_j \leq E, \quad \forall j \in \mathcal{I} \bigcup \{r(w)\}, (i,j) \in \mathcal{A}, w \in \mathcal{W} \tag{22}$$

$$\sum_{(i,j)\in\mathcal{A}} l_{ij} x^w_{ij} \leq L^w + \eta^w, \quad \forall w \in \mathcal{W} \tag{23}$$

$$e^w_{r(w)} \leq E_o, \quad \forall w \in \mathcal{W} \tag{24}$$

$$e^w_{s(w)} \geq E_D, \quad \forall w \in \mathcal{W} \tag{25}$$

$$x^w_{ij} \in \{0,1\}, \quad \forall (i,j) \in \mathcal{A}, w \in \mathcal{W} \tag{26}$$

$$y_i \in \{0,1\}, \quad \forall i \in \mathcal{I} \tag{27}$$

The objective function shown by Eq. (13) is the sum of the total range anxiety and a big-M component. As our priority in determining the EV charging station deployment is to refuel as many flows as possible, the uncovered demand is penalized by the big-M component in the objective function. The value of M should be sufficiently large in order to avoid the case that the EVs of an OD pair travel on the auxiliary link (i.e., not covered) at an optimal solution although they are actually able to be refueled by the constructed stations. A safe value should thus be no less than the maximal accumulated range anxiety of a trip, i.e., $M \geq \bar{R}_{\max} \left\lfloor B / \min_{i \in \mathcal{I}} \{c_i\} \right\rfloor$, where $\bar{R}_{\max}$ represents the maximal accumulated range anxiety experienced by an EV driver over a path segment with the final SOC being 0, and $\left\lfloor B / \min_{i \in \mathcal{I}} \{c_i\} \right\rfloor$ is the upper bound of the station number. Constraint (14) is the flow conservation equation for each OD pair. Constraint (15) restricts the total budget for the EV charging station deployment. Eqs. (16)-(18) are the constraints for the feasible charging logic and have been justified in Subsection 2.1. Specifically, Constraints (16)-(17) update the SOC at the traversed nodes along a trip. If $x_{ij}^w = 1$, Constraint (16) reduces to $e_j^w \leq e_i^w - d_{ij} + Ey_j$, which will become binding at an optimal solution when $y_j = 0$, and redundant when $y_j = 1$. If, on the contrary, $x_{ij}^w = 0$, Constraint (16) will reduce to a redundant constraint $e_j^w \leq e_i^w + E(1 + y_j)$ whatever the value of y_j is. Constraint (17) requires that the SOC is reset to E after traversing a built EV charging station. Constraint (18) ensures the range feasibility of traversed link along a trip. For a link terminating at an ordinary node of the network, i.e., $j \in \mathcal{N} \setminus \mathcal{I}$, Constraints (16) and (17) reduce to Constraints (19) and (20). Constraints (21) and (22) jointly set the upper bound of the final SOC at the end node of each path segment over a trip, i.e., the SOC upon arriving an EV charging station or a destination, and will be binding at an optimal solution with $r_j^w = e_i^w - d_{ij}$ when $x_{ij}^w = 1$, and $r_j^w \geq E_{comf}$ otherwise. Eq. (23) imposes the distance constraint for a deviation path. Constraints (24) and (25) are the SOC requirements for the EVs before departure and after arrival, respectively. They are valid if the origins of the OD pairs are not candidate locations, i.e., $\mathcal{I} \cap \{r(w)\}_{w \in \mathcal{W}} = \varnothing$; otherwise, an auxiliary copy of the underlying origin node connected to the correspondent original origin node by a link with zero length and electricity consumption should be added to the network. Constraints (26) and (27) define the decision variables as binary variables.

3.2 Model properties

Unlike the existing path or combination based FRLM and RFRLM model, whose size is largely determined by the detour tolerance and driving range of EV, and can easily become overwhelming even for a small network, our model is compact in the sense that it has a polynomial number of constraints, and its size is fixed for a network. Since we have explicitly modeled the charging logic and range feasibility in the model, path or combination pre-generation is not required for model formulation, and more importantly, when implemented in the numerical experiments the model is not likely to have the out-of-memory issue confronted by RFRLM (Kim and Kuby, 2012). Another merit of the proposed model is its flexibility to encompass special cases and incorporate other aspects such as station capacity and multiple types of EV drivers with different range anxiety profiles, etc. For example, the model can be easily modified to be a maximum flow model by replacing the objective function in Eq. (13) by $\sum_{w\in\mathcal{W}} f^w x^w_{r(w)s(w)}$. A set covering model can also be obtained by revising the objective function to be $\sum_{i\in\mathcal{I}} c_i y_i$ and removing the budget constraint and the auxiliary links in the network. Moreover, the model can be modified to be a min-max regret model if minimizing the flow weighted maximal range anxiety of EV drivers (corresponding to the worst-case scenario) is the major concern of the EV charging station deployment. In this case, the objective function will become $\min_{\mathbf{x},\mathbf{y},\mathbf{e},\mathbf{r}} \sum_{w\in\mathcal{W}} \left[f^w \max_j \{F(r^w_j)\} \right]$ where $F(\bullet)$ denotes the function of range anxiety with respect to SOC.

Despite the above merits, the bilinear term $\bar{R}(r^w_j)y_j$ and the nonlinearity of the integral in the expression of $\bar{R}(r)$ in Eq. (13), however, make the model not easily solvable by commercial solvers. Luckily, we find that the bilinear terms can be linearized by replacing each $\bar{R}(r^w_j)y_j$ in the objective function (13) with a new variable Q^w_j and imposing a new set of constraints that enforces $Q^w_j = \bar{R}(r^w_j)y_j$ at an optimal solution:

$$Q^w_j \ge \bar{R}(r^w_j) + \bar{R}_{\max}(y_j - 1) \tag{28}$$

$$Q^w_j \ge 0 \tag{29}$$

where $\bar{R}_{\max}$ is the maximal accumulated range anxiety over a path segment and is bounded by $\bar{R}(0)$. Moreover, the following proposition demonstrates that, after linearization, the resultant model [DCSP] would be a mixed-integer convex programming model such that it can be approximated by a MILP model using the outer-approximation algorithm detailed in the next subsection.

Proposition 1. Model [DCSP] is a mixed-integer convex programming model if the range anxiety profile $R(t)$ is differentiable.

Proof. By taking the second derivative of $\bar{R}(r)$, we obtain

$$\bar{R}''(r) = R'(S^{-1}(r)) \cdot \left[S^{-1\prime}(r) \right]^2 + R(S^{-1}(r)) \cdot S^{-1\prime\prime}(r) \tag{30}$$

Since $S(\bullet)$ is a linearly decreasing function, its inverse function $S^{-1}(\bullet)$ will also be a linearly decreasing function. In other words, we have $S^{-1\prime}(r) \geq 0$ and $S^{-1\prime\prime}(r) = 0$. In addition, as $R(\bullet)$ is an increasing and differentiable function, we have $R'(\bullet) \geq 0$. Hence it follows from Eq. (30) that $\bar{R}''(r) \geq 0$, implying that $\bar{R}(r)$ is a convex function. Because the nonnegative weighted sum in the objective function of the model [DCSP] is an operation that preserves convexity, we can conclude that the model [DCSP] is a mixed-integer convex programming model. □

4. Outer-approximation Algorithm

The outer-approximation algorithm was initially proposed by Duran and Grossmann (1986) to obtain an ε-optimal solution to mixed-integer programming models with nonlinear inequalities such that the difference between the obtained objective function value and the optimal objective function value is within the exogenously given tolerance $\varepsilon > 0$. This method has been extended and applied in many research disciplines such as the chemical engineering and process design (Grossmann and Kravanja, 1995; Varvarezos et al., 1992), sailing speed optimization and revenue management in liner shipping studies (Wang and Meng, 2012; Wang et al., 2015), and a recent service pricing problem in an electric shared mobility system (Xu et al., 2018). The outer-approximation algorithm can handle general mixed-integer nonlinear programming problems with convex terms both in the objective function and constraints such as the model [DCSP]. In particular, the model [DCSP] will be transformed into a MILP model by approximating the convex terms in both the objective function and constraints with multiple linear functions. The resultant MILP problem can then be solved readily by state-of-the-art MILP solvers like CPLEX.

To apply the outer-approximation algorithm, the model [DCSP] should be first rewritten as follows by introducing an auxiliary continuous variable B_j^w, $\forall j \in \mathcal{I} \cup \{r(w)\}, w \in \mathcal{W}$ as a proxy variable for the nonlinear term $\bar{R}(r_j^w)$ in the objective function (13) and Constraint (28):

$$\min_{\mathbf{Q},\mathbf{B},\mathbf{x},\mathbf{y},\mathbf{e},\mathbf{r}} Obj^I(\mathbf{Q},\mathbf{B},\mathbf{x},\mathbf{y},\mathbf{e},\mathbf{r}) = \sum_{w \in \mathcal{W}} f^w \left[\sum_{j \in \mathcal{I}} Q_j^w + B_{s(w)}^w \right] + M \sum_{w \in \mathcal{W}} f^w x_{r(w)s(w)}^w \quad (31)$$

subject to Constraints (14)-(27), (29), and

$$Q_j^w \geq B_j^w + \bar{R}_{\max}(y_j - 1), \quad \forall j \in \mathcal{I}, w \in \mathcal{W} \quad (32)$$

$$B_j^w \geq \bar{R}(r_j^w), \quad \forall j \in \mathcal{I} \cup \{s(w)\}, w \in \mathcal{W} \quad (33)$$

Constraint (33) can thereby be relaxed by replacing the function $\bar{R}(r_j^w)$ with many linear functions being tangent to the convex curve $\bar{R}(r_j^w)$ as illustrated in Figure 6. Those linear functions can be interpreted as the underestimated accumulated range anxiety and are grouped into a set represented by $\mathcal{K} = \{1, 2, ..., K-1, K\}$. Let $a_j^{w(k)}$ and $b_j^{w(k)}$ denote the slope and intercept of the k^{th} tangent line of the curve $\bar{R}(r_j^w)$ at a point $r_j^{w(k)}$, respectively. The original constraint (33) is relaxed to be

$$B_j^w \geq a_j^{w(k)} r_j^w + b_j^{w(k)}, \quad \forall j \in \mathcal{I} \cup \{s(w)\}, w \in \mathcal{W}, k \in \mathcal{K} \quad (34)$$

where $a_j^{w(k)} = \bar{R}'(r_j^{w(k)})$ and $b_j^{w(k)} = \bar{R}(r_j^{w(k)}) - \bar{R}'(r_j^{w(k)}) r_j^{w(k)}$. The resultant MILP model is thus formulated by

[DCSP -II]

$$\min_{\mathbf{Q},\mathbf{B},\mathbf{x},\mathbf{y},\mathbf{e},\mathbf{r}} Obj^{II}(\mathbf{Q},\mathbf{B},\mathbf{x},\mathbf{y},\mathbf{e},\mathbf{r}) \quad (35)$$

subject to Eqs. (14)-(27), (29), (32), and (34).

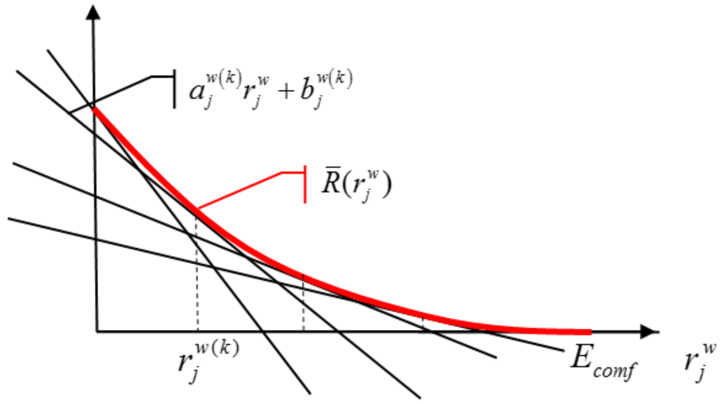

Figure 6. Illustration of linear approximation for Constraint (33)

It can be seen that model [DCSP-II] is a relaxation of model [DCSP] because the values of Q_j^w and $\bar{R}(r_{s(w)}^w)$ in the objective function are underestimated. Therefore its solution provides a lower bound for the optimal solution of the model [DCSP] as demonstrated in the following proposition:

Proposition 2: Let $(\mathbf{Q}^*, \mathbf{B}^*, \mathbf{x}^*, \mathbf{y}^*, \mathbf{e}^*, \mathbf{r}^*)$ denote an optimal solution to the MILP model [DCSP-II] and Obj^* denote the optimal objective value of mixed-integer convex programming model [DCSP]. Then we have

$$Obj^{II}(\mathbf{Q}^*, \mathbf{B}^*, \mathbf{x}^*, \mathbf{y}^*, \mathbf{e}^*, \mathbf{r}^*) \le Obj^* \le Obj(\mathbf{x}^*, \mathbf{y}^*, \mathbf{e}^*, \mathbf{r}^*) \tag{36}$$

Let $\hat{R}(r_j^w) = \max_{k \in \mathcal{K}} \left\{ a_j^{w(k)} r_j^w + b_j^{w(k)} \right\}$ denote the piecewise linear approximation function for $\bar{R}(r_j^w)$. The approximation error of the optimal solution can be controlled within a pre-specified tolerance $\varepsilon > 0$ by properly generating a sufficient number of tangent lines such that the approximation error for Constraint (33), i.e., $\bar{R}(r_j^w) - \hat{R}(r_j^w)$, is no larger than $\hat{\varepsilon} = \dfrac{\varepsilon}{(|\mathcal{I}|+1) \cdot |\mathcal{W}|}$. In other words, if $\bar{R}(r_j^w) - \hat{\varepsilon} \le \hat{R}(r_j^w) \le \bar{R}(r_j^w), \forall j \in \mathcal{I} \cup \{s(w)\}, w \in \mathcal{W}$, we have the following inequality:

$$Obj(\mathbf{x}^*, \mathbf{y}^*, \mathbf{e}^*, \mathbf{r}^*) - Obj^{II}(\mathbf{Q}^*, \mathbf{B}^*, \mathbf{x}^*, \mathbf{y}^*, \mathbf{e}^*, \mathbf{r}^*) \le \varepsilon \tag{37}$$

Eqs. (36) and (37) jointly imply that the proposed outer-approximation algorithm can obtain the ε-optimal solution to the model [DCSP], as summarized in the following proposition:

Proposition 3: For any exogenously required tolerance $\varepsilon > 0$, the outer-approximation algorithm can obtain the ε-optimal solution to the model [DCSP], i.e.,

$$Obj(\mathbf{x}^*,\mathbf{y}^*,\mathbf{e}^*,\mathbf{r}^*)-\varepsilon \le Obj^* \le Obj(\mathbf{x}^*,\mathbf{y}^*,\mathbf{e}^*,\mathbf{r}^*) \tag{38}$$

if we choose an error bound $\hat{\varepsilon}$ for the tangent line generation such that $\hat{\varepsilon} \le \dfrac{\varepsilon}{(|\mathcal{I}|+1)\cdot|\mathcal{W}|}$.

Given the tolerance $\hat{\varepsilon} > 0$ to approximate the convex function $\bar{R}(r_j^w)$ in a domain $r_j^w \in \left[r_j^{w(L)}, r_j^{w(U)}\right]$, the set of tangent points for tangent line generation denoted by $\mathbf{E} = \left\{r_j^{w(k)}, k \in \mathcal{K}\right\}$ can be obtained by the following pseudo-code:

Pseudo-code 1: Finding the set of break points for tangent line generation.

Initialize $\mathbf{E} \leftarrow \{r_j^{w(L)}, r_j^{w(U)}\}$;
Function [$\mathbf{E}$]=*FindTangentPoint* $(r_j^{w(L)}, r_j^{w(U)}, \mathbf{E})$
    $[a_1, b_1]$=*TangentLine* ($r_j^{w(L)}$);
    $[a_2, b_2]$=*TangentLine* ($r_j^{w(U)}$);
    [$r_j^w, \hat{R}(r_j^w)$]=*Intersection* (a_1, b_1, a_2, b_2); Error= $\bar{R}(r_j^w) - \hat{R}(r_j^w)$;
    If Error> $\hat{\varepsilon}$, Then
        $\mathbf{E} \leftarrow r_j^w$;
        [$\mathbf{E}$]=*FindTangentPoint* $(r_j^{w(L)}, r_j^w, \mathbf{E})$
        [$\mathbf{E}$]=*FindTangentPoint* $(r_j^w, r_j^{w(U)}, \mathbf{E})$
    End if
End function

Note that *FindTangentPoint* in the above pseudo-code is the recursive function to find the set of tangent points of the tangent lines. In each recursion step, it returns the unique tangent point in the domain $\left[r_j^{w(L)}, r_j^{w(U)}\right]$ with the maximum error for approximating the convex function $\bar{R}(r_j^w)$ using the outer-approximation envelope formulated by the two tangent lines at the two end points of the interval. Given a specific value of r_j^w, *TangentLine* is a sub-function to return the slope and intercept of the tangent line for the convex curve $\bar{R}(r_j^w)$ at a point $\left(r_j^w, \bar{R}(r_j^w)\right)$. *Intersection* is the sub-function that returns the coordinate value of the intersection of two lines given their slopes and intercepts. Since it holds that $\bar{R}(r_j^w) = 0$ for any $r_j^w \in \left[E_{comf}, E\right]$ in this study, we only need to generate the tangent points in the domain $r_j^w \in \left[0, E_{comf}\right]$.

5. Model Extension

The model presented in Section 3 is a direct extension to RFLM and DRFLM by incorporating the range anxiety of travellers in the determination of EV charging station deployment. The additional costs incurred by making a stop and/or waiting for recharge to complete are not considered. This section presents a more general model on top of model [DCSP] that incorporates the charging impedance, e.g., the cost and the time required for charging. As such, in addition to the parameters and variables introduced previously, we define another binary decision variable for each OD pair, i.e., y_i^w, $\forall i \in \mathcal{I}, w \in \mathcal{W}$, denoting whether the travelers of OD pair w will charge at the station i. The problem of finding the optimal deployment of EV charging stations considering the charging impedance, referred to as DCSPCI, can thus be formulated by replacing y_i in Eqs. (13), (16), and (17) with y_i^w, including an additional term representing the total incurred charging impedance along a path on the left hand of Eq. (23), and imposing a constraint linking y_i^w and y_i. We consider a general charging impedance consisting of two components that are charging-amount-independent (e.g., the impedance of making a stop) and charging-amount-dependent (e.g., charging time and cost) respectively. Particularly, the additional term added to Eq. (23) is given by $\sum_{i \in \mathcal{I}} [\alpha_i y_i^w + \beta_i (E - r_i^w) y_i^w]$, where α_i denotes the average charging impedance incurred at station i that is independent of the charging amount, and β_i denotes the charging-amount-dependent impedance incurred at station i per unit amount of charging. In summary, the considered problem can be formulated as follows:

[DCSPCI]

$$\min_{\mathbf{x},\mathbf{y},\mathbf{e},\mathbf{r}} \quad Obj^{CI}(\mathbf{x},\mathbf{y},\mathbf{e},\mathbf{r}) = \sum_{w \in \mathcal{W}} f^w \left[\sum_{j \in \mathcal{I}} \bar{R}(r_j^w) y_j^w + \bar{R}(r_{s(w)}^w) \right] + M \sum_{w \in \mathcal{W}} f^w x_{r(w)s(w)}^w \tag{39}$$

subject to Eqs. (14), (15), (18)-(22), (24)-(27), and

$$e_j^w \le e_i^w - d_{ij} x_{ij}^w + E(1 - x_{ij}^w + y_j^w), \quad \forall j \in \mathcal{I}, (i,j) \in \mathcal{A}, w \in \mathcal{W} \tag{40}$$

$$E y_j^w \le e_j^w \le E, \quad \forall j \in \mathcal{I}, w \in \mathcal{W} \tag{41}$$

$$\sum_{i \in \mathcal{I}} [\alpha_i y_i^w + \beta_i (E - r_i^w) y_i^w] + \sum_{(i,j) \in \mathcal{A}} l_{ij} x_{ij}^w \le L^w + \eta^w, \quad \forall w \in \mathcal{W} \tag{42}$$

$$y_i^w \le y_i, \quad \forall i \in \mathcal{I} \tag{43}$$

$$y_i^w \in \{0,1\}, \quad \forall i \in \mathcal{I} \tag{44}$$

It can be seen that the charging-amount-dependent charging impedance in Eq. (42) is a bilinear term. By a similar method in Section 3.2, we define a new continuous variable P_i^w, $\forall i \in \mathcal{I}, w \in \mathcal{W}$ to replace $(E - r_i^w) y_i^w$ in Eq. (42) and impose a new set of constraints that enforce $P_i^w = (E - r_i^w) y_i^w$ at an optimal solution:

$$P_i^w \le E y_i^w, \quad \forall i \in \mathcal{I}, w \in \mathcal{W} \tag{45}$$

$$P_i^w \le E - r_i^w, \quad \forall i \in \mathcal{I}, w \in \mathcal{W} \tag{46}$$

$$P_i^w \ge E y_i^w - r_i^w, \quad \forall i \in \mathcal{I}, w \in \mathcal{W} \tag{47}$$

$$P_i^w \ge 0, \quad \forall i \in \mathcal{I}, w \in \mathcal{W} \tag{48}$$

We can find that the incorporation of charging impedance does not affect the model property and Proposition 1 is still valid. Therefore, the proposed outer-approximation algorithm is applicable. The ε-optimal solution to the model [DCSPCI] can be found by solving the following MILP model:

[DCSPCI-I]

$$\min_{\mathbf{Q},\mathbf{B},\mathbf{P},\mathbf{x},\mathbf{y},\mathbf{e},\mathbf{r}} \quad Obj^{CI-I}(\mathbf{Q},\mathbf{B},\mathbf{P},\mathbf{x},\mathbf{y},\mathbf{e},\mathbf{r}) = \sum_{w \in \mathcal{W}} f^w \left[\sum_{j \in \mathcal{I}} Q_j^w + B_{s(w)}^w \right] + M \sum_{w \in \mathcal{W}} f^w x_{r(w)s(w)}^w \tag{49}$$

subject to Eqs. (14), (15), (18)-(22), (24)-(27), (29), (34), (40), (41), (43), (44)-(48), and

$$\sum_{i \in \mathcal{I}} [\alpha_i y_i^w + \beta_i P_i^w] + \sum_{(i,j) \in \mathcal{A}} l_{ij} x_{ij}^w \le L^w + \eta^w, \quad \forall w \in \mathcal{W} \tag{50}$$

$$Q_j^w \ge B_j^w + \bar{R}_{\max} (y_j^w - 1), \quad \forall j \in \mathcal{I}, w \in \mathcal{W} \tag{51}$$

6. Numerical Experiments

This section presents the numerical experiments to evaluate the performance of the proposed model and outer-approximation algorithm. The algorithm is coded in C++ calling IBM ILOG CPLEX 12.6 on a personal computer with Intel Core i7 3.6 GHz CPU with 16 GB RAM. Two network topologies, i.e., a benchmark 25-node network and a real-life Texas highway network, will be used. We will first examine the computational performance of the proposed models, especially the effect of pre-specified tolerance $\hat{\varepsilon}$ on the performance of the proposed algorithm, in both networks. After that, the benefit of incorporating range anxiety in the decision-making for EV charging station deployment will be demonstrated in comparison with the maximum flow model. We will also compare the solutions of the original model and the extended model that considers the charging impedance. Finally, sensitivity analysis of several parameters on the system performance and the impact analysis of considering only a subset of OD pairs will be conducted to derive practical insights.

6.1 Networks and parameter setting

The first network is a hypothetical network consisting of 25 nodes and 86 links (43 undirected edges) in Figure 7. This network has been used by many scholars in the studies for refueling station location optimization (Kim and Kuby, 2012; MirHassani and Ebrazi, 2012; Yıldız et al., 2016). The link length shown beside each edge in Figure 7 is adopted from Kim and Kuby (2012). The electricity consumption of a link (i, j), measured in kWh, is chosen as a uniformly random integer from the set $\{3, 4, 5, ..., 9\}$. All nodes will be considered as origins, destinations, and candidate locations of EV charging stations, leading to a total of 300 OD pairs and 25 candidate locations, respectively. The traffic flow for each OD pair is estimated by the gravity model (Hodgson, 1990).

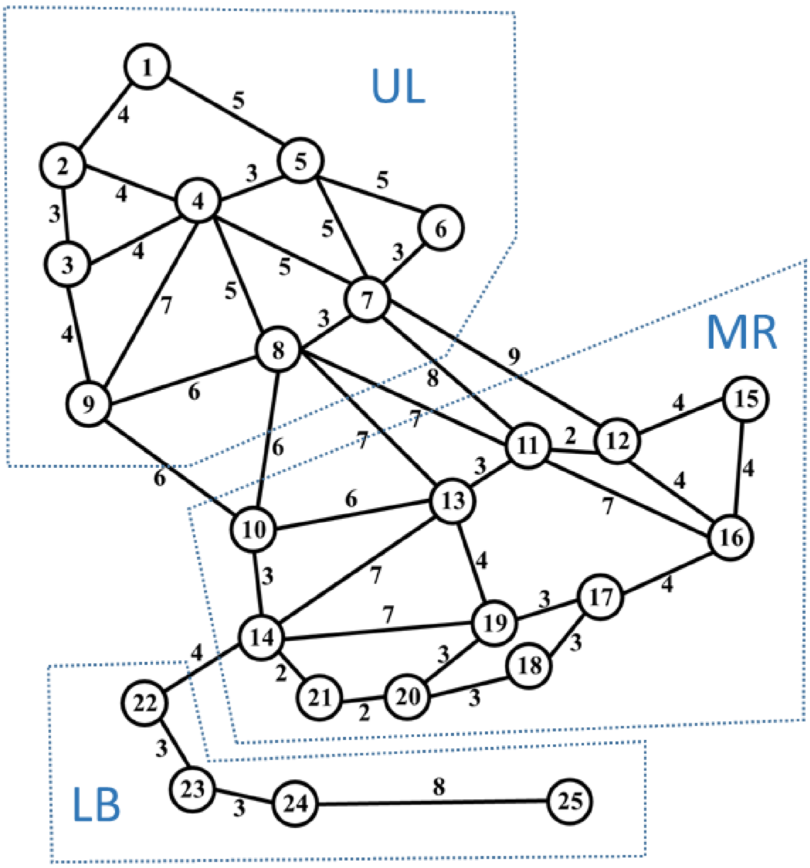

Figure 7. A hypothetical 25-node network

The other network is a real-life Texas highway network created by Lee and Han (2017). As shown in Figure 8, this highway network consists of 124 nodes and 238 edges (476 links), and has been used for an EV charging station location problem in Lee and Han (2017) under probabilistic travel range. The link length shown beside each edge in Figure 8 is also adopted from Lee and Han (2017), with a nominal value of 10 representing 250 km in reality. EVs are assumed to be the second-generation Nissan Leaf 40 kWh with a range of 243 km (Nissan, 2019). The electricity consumption measured in kWh, is chosen as a uniformly random integer with a maximum of 5 kWh deviation from the value estimated by the particulars of Nissan Leaf 40 kWh. Considering the 30 largest cities of Texas (see the filled rectangular nodes in Figure 8) as origins or destinations results in a total of 435 OD pairs. All nodes are considered as candidate EV charging station locations. The traffic flow between each OD pair is again obtained by the gravity model using the population of a city as weight.

Figure 8. The Texas highway network (Yıldız et al., 2016)

For both networks, we assume for simplicity that the construction cost of each station is 1, i.e., $c_i = 1, \forall i \in \mathcal{I}$. Following the convention in the literature, the initial and final SOC threshold of the EVs at their origins and destinations are assumed to be half of the correspondent usable battery capacity, i.e., $E_O = E_D = \frac{1}{2}E$. Regarding the profile of range anxiety, let a denote the unit discharging rate of the battery, and $t^* := \frac{E - E_{comf}}{a}$ be the critical time epon that a driver with a fully charged EV starts suffering from range anxiety. We assume that the range anxiety profile of EV drivers over a single path segment follows a convex piece-wise polynomial function expressed by

$$R(t) = \begin{cases} 0, \quad if \ 0 \le t < t^* \\ \dfrac{R_{\max}}{(E/a - t^*)^2}(t - t^*)^2, \quad if \ t^* \le t \le E/a \end{cases} \tag{52}$$

By simple manipulation, we obtain the function of the accumulated range anxiety as follows:

$$\bar{R}(r) = \begin{cases} 0, \quad if \ E_{comf} < r \le E \\ \dfrac{R_{\max}}{3aE_{comf}{}^2}(E_{comf} - r)^3, \quad if \ 0 \le r \le E_{comf} \end{cases} \tag{53}$$

The maximal accumulated range anxiety achieved at $r = 0$ would be $\bar{R}_{\max} = \frac{R_{\max} E_{comf}}{3a}$. For simplicity, the discharging rate of the battery is assumed to be 1, and E_{comf} is assumed to be half of the usable battery capacity. Unless stated otherwise, $R_{\max}$ is normalized to be 100% throughout the numerical experiments. The baseline values of these parameters are presented in Table 1.

Table 1. Baseline values of parameters used in numerical experiments

6.2 Algorithm performance

To examine the effect of pre-specified tolerance $\hat{\varepsilon}$ on the performance of the proposed outer-approximation algorithm in terms of solution quality and computational efficiency, we will first solve the DCSP under different values of $\hat{\varepsilon}$ in the benchmark 25-node network. Given a particular $\hat{\varepsilon}$, ten instances with different combinations of parameters regarding the budget, the battery capacity, and the path deviation tolerance, i.e., $B \in \{1, 2, ..., 25\}$, $E \in \{6, 7, 8, 9, 10\}$, and $\eta^w \in \{0, 10\%L^w, 20\%L^w, 30\%L^w, 40\%L^w\}$, will be randomly generated, and the average results are reported. We also apply the parallel optimization mode of IBM ILOG CPLEX 12.6 to improve computational efficiency. The ratio of elapsed time to CPU time is also reported.

Table 1 shows the results of the outer-approximation algorithm under different values of $\hat{\varepsilon}$ ranging from 0.01 to 0.5 in the 25-node network. Overall, it shows that for any scenario, the proposed method obtains the ε-optimal solutions within 63 seconds, and the elapsed time averaged over all scenarios is 35.57 seconds. This outcome reveals the efficiency of the proposed algorithm and its potential to be implemented in a real-world transportation network. In addition, the average relative gap is only 0.005, and the value of $\hat{\varepsilon} = 0.01$ is sufficient enough to achieve a near-optimal solution with a relative gap less than 0.001. We further visualize the variations of the gap and elapsed time with the increase of tolerance $\hat{\varepsilon}$ in Figure 9. It shows that instead of increasing steadily with a growing value of tolerance, the variation of gap somehow follows a step-wise pattern. For example, the gap has been increased by more than 70 when the value of $\hat{\varepsilon}$ increases from 0.01 to 0.03, whereas the increment has dramatically decreased to be less than 35 when the value of $\hat{\varepsilon}$ increases from 0.03 to 0.1. On average the instances with $\hat{\varepsilon} = 0.5$ run the shortest computation time, while those with $\hat{\varepsilon} = 0.01$ take the longest time among all scenarios. The time difference is more than 40 seconds, almost double the time under $\hat{\varepsilon} = 0.5$. The findings show in general terms that the computational efficiency of the outer-approximation method is positively and largely affected by the tolerance $\hat{\varepsilon}$. This is consistent with our expectation that a smaller tolerance $\hat{\varepsilon}$ indicates more additional constraints, i.e., Eq. (34), to be generated, more time to solve the linear programming relaxation problem, and thereby more time to solve the model [OP-II] by B&B algorithm. The trade-off between solution quality and computational efficiency should thus be well balanced by fine-toning the value of $\hat{\varepsilon}$ in real applications. The time ratio in the last column of Table 1 is averaged to be 4.49, demonstrating the competence of the parallel optimization in CPLEX to reduce the computational time of the proposed model.

Table 1. Results of the proposed outer-approximation algorithm in 25-node network under different tolerance $\hat{\varepsilon}$

$\hat{\varepsilon}$	UB	LB	Gap	Relative Gap =Gap/UB	Elapsed Time (s)	CPU Time (s)	Time Ratio
0.01	77,408	77,378	30	0.000	62.18	306.97	4.94
0.03	77,428	77,320	108	0.001	44.27	199.11	4.50

0.05	77,442	77,319	123	0.002	44.04	223.50	5.07
0.07	77,442	77,319	123	0.002	36.87	173.55	4.71
0.09	77,451	77,315	136	0.002	36.82	171.10	4.65
0.1	77,446	77,306	140	0.002	31.73	132.59	4.18
0.2	77,617	77,177	440	0.006	28.19	123.79	4.39
0.3	77,546	77,052	494	0.006	26.11	107.27	4.11
0.4	77,726	76,847	878	0.011	23.74	96.72	4.07
0.5	78,382	76,640	1,742	0.022	21.78	93.29	4.28
Maximum	--	--	1,742	0.022	62.18	306.97	5.07
Average	77,589	77,167	422	0.005	35.57	162.79	4.49

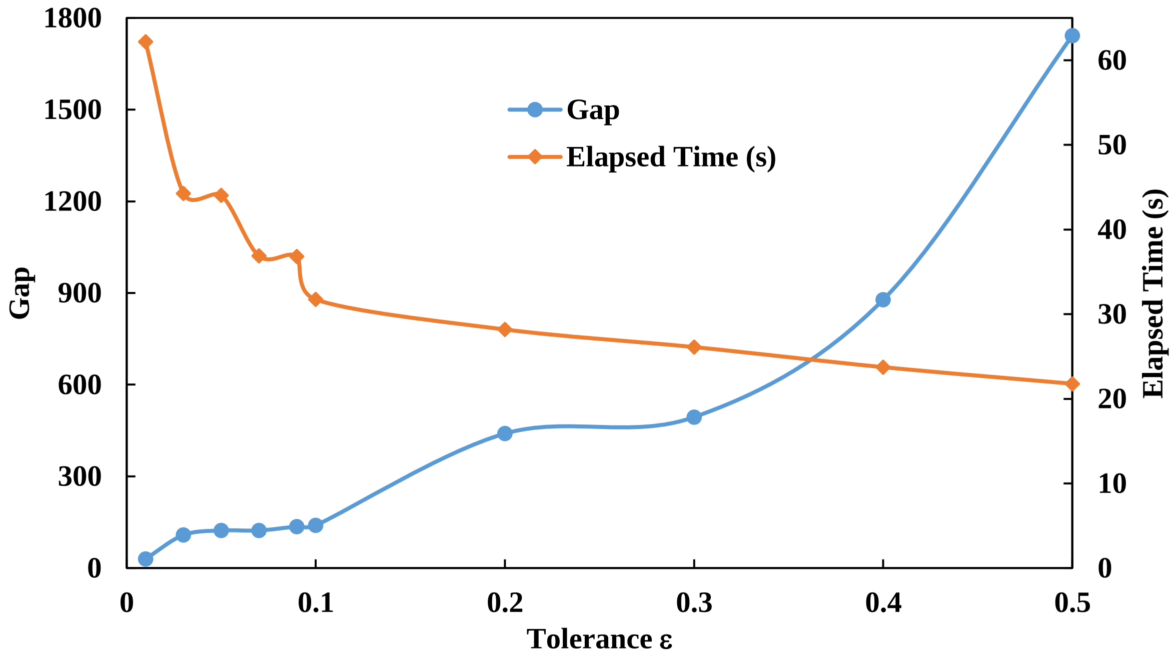

Figure 9. Variations of the gap and elapsed time with the increase of tolerance $\hat{\varepsilon}$

To further examine its scalability to large networks, we apply the proposed outer-approximation algorithm in the Texas highway network. A total of 30 problem instances are created by considering 3 levels of path deviation tolerance, i.e., $\eta \in \{0, 5\%L^w, 10\%L^w\}$, and 10 values of budget, i.e., 5, 10, …, 50. We report in Table 2 the covered flow ratio (CFR) and the elapsed time for solving each instance. For problem instances that are not solved to optimality within 3 hours, we will present the absolute optimality gap (GAP_{abs}), i.e., the difference of incumbent solution and the lower bound obtained within 3 hours. Kindly note that the default stopping criteria of the algorithm in CPLEX in terms of the absolute optimality gap is 10^{-6}. The parameter $\hat{\varepsilon}$ in the proposed outer-approximation algorithm is set to 0.01. The parallel mode of CPLEX is turned on to reduce the computation time.

Table 2 shows that compared with the small network, the runtime of the solution approach has tremendously increased in a large network, and more than half of the instances cannot be solved to optimality within 3 hours. Since the model size is determined by the size of the network and OD pairs, it definitely takes a much longer time to solve the proposed model. In addition, it is worthwhile to note that although the proposed approach does not require path generation and the model size has nothing to do with the path deviation tolerance (note that the value of path deviation tolerance only affects Constraint (23)), the solution time also obviously increases with the path deviation tolerance. This phenomenon is quite similar to the solution approaches entailing path generation (Yıldız et al., 2016). It may be attributed to a larger feasible solution space allowed by a larger path deviation tolerance. The low computational efficiency of the model and solution approach in the Texas highway network demonstrates the necessity to develop more efficient methods for implementation in large-scale problems. Though computational intensive, it manages to solve 10 problem instances within 3 hours, and the memory issue confronted by the path and charging combination pre-generation in RFRLM (Kim and Kuby, 2012) is not a big problem. The average optimality gap is 0.0080. For the instances that are not solved to optimality, the optimality gap is no more than 0.0385, and the most computationally extensive instances seems always associated with the budget being around 20. Although some instances (see the instances in bold in Table 2), e.g., the instance with $B = 40$ and $\eta = 0$ are not solved to optimality within the time limit, their solution can be deemed as the optimal because further increase of the budget does not result in the growth of covered flow (Note that the instance with $B = 45$ and $\eta = 0$ are solved to optimality). More importantly, we find from supplementary numerical experiments that lengthening the solution time limit marginally contributes to the flow coverage and optimality gap closure. For example, the covered flow ratio for the problem instance with $B = 25$ and $\eta = 0$ increases slightly from 0.95 to 0.96 when the solution time threshold is extended from 3 hrs to 10 hrs. This, to some extent, suggests that we may as well accept the incumbent non-optimal solution since the additional computational cost to achieve a better solution, though only slight improvement in solution quality, can be prohibitively tremendous. Another more convincing reason is that these solutions are actually quite near to the optimal solution.

Table 2. Performance of the proposed outer-approximation algorithm in Texas highway network

B	$\eta = 0$	$\eta = 5\% L^w$	$\eta = 10\% L^w$

	CFR	GAP$_{abs}$	Elapsed Time (s)	CFR	GAP$_{abs}$	Elapsed Time (s)	CFR	GAP$_{abs}$	Elapsed Time (s)
5	0.74	0	1,536	0.74	0	1,539	0.76	0.0041	10,800
10	0.87	0	1,518	0.87	0	2,702	0.87	0.0157	10,800
15	0.91	0	7,615	0.91	0.0079	10,800	0.91	0.0313	10,800
20	0.94	0.0055	10,800	0.93	0.0229	10,800	0.93	0.0385	10,800
25	0.95	0.0157	10,800	0.95	0.0149	10,800	0.95	0.0272	10,800
30	0.96	0.0129	10,800	0.96	0.0106	10,800	0.96	0.0178	10,800
35	0.97	0.0011	10,800	0.97	0.0121	10,800	**0.98**	**0.0012**	**10,800**
40	**0.98**	**0.0002**	**10,800**	**0.98**	**0.0001**	**10,800**	**0.98**	**0.0001**	**10,800**
45	0.98	0	3,491	0.98	0	5,331	0.98	0.0014	10,800
50	0.98	0	2,420	0.98	0	1,295	0.98	0	4,629

Remark: instances in bold are actually solved to optimality although they have positive gaps.

6.3 Results comparison to the maximum flow model

To numerically justify the benefit of minimizing the range anxiety of EV drivers for EV charging station location optimization, we compare the optimal station location (Location No.) and covered flow ratios (CFR) obtained by solving the proposed model and the maximum flow model under the same parameter setting in 25-node network, i.e., $B \in \{1, 2, ..., 25\}$, $E = 8$, and $\eta^w = 0$. We also report the number of different locations resulted from the two models. Since $\hat{\varepsilon} = 0.01$ appears small enough to offer a near-optimal solution within an acceptable elapsed time, the outer-approximation algorithm with $\hat{\varepsilon} = 0.01$ will be employed to carry out the following analyses. The results are tabulated in Table 3. We can see that both models cover the same traffic flow in all instances. Although the proposed model aims to minimize the range anxiety of EV drivers, the big-M coefficient for the uncovered flow component forces the model to cover as many flows as possible. As for the station deployment, the locations suggested by the two models are identical in many instances. There are, however, a few exceptions under budget 1, 9, 15, 21, and 23 with three different number of stations at maximum, where the proposed model does provide a more sensible station deployment that alleviates the range anxiety of travelers while covering the same amount of traffic flow. For instance, under $B = 1$, although both models cover the same traffic flow from origin node 19 to the destination node 20, they suggest different station location at node 20 and 19 respectively. It can be checked that either node 20 or node 19 can ensure the successful travel of EV drivers from origin node 19 to the destination node 20 without getting stranded halfway, whereas the range anxiety can be wholly eliminated by establishing an EV charging station at node 19 in contrast to node 20. The numerical results, together with the previous example in Figure 1, validate the significance of this study.

6.4 Results comparison to the extended model

To explore how the incorporation of charging impedance influence the EV charging station deployment and flow coverage, we compare the optimal station location (Location No.) and covered flow ratios (CFR) obtained by solving the original model [DCSP] and the extended model [DCSPCI] under the same parameter setting in the 25-node network, i.e., $B \in \{1, 2, ..., 25\}$, $E = 8$, and $\eta^w = 20\% L^w$. Again we set $\hat{\varepsilon} = 0.01$ in the outer-approximation algorithm to obtain the near-optimal solution. The parameters in the charging impedance function, i.e., α_i and β_i, are set to be 0.05 and 0.1, respectively. The results are shown in Table 4. We can see that the charging impedance does greatly reduce the flow coverage because the detour distance together with the total charging impedance can easily exceed the drivers' path deviation tolerance, thus making some range-feasible paths and charging patterns unfavourable. Moreover, it appears that the increase of budget amplifies the negative effect of charging impedance on flow coverage as the difference of covered flow ratios increases steadily from 0 to 3.4 when the budget grows from 1 to 25. As for the station deployment, the optimal locations obtained from the two models are different in all instances except the first two and the last two instances. It seems that the effect of charging impedance on station deployment measured by number of different station locations will first increase with the budget and after reaching the maximal different number of stations, i.e., six, under the budget of 12, the difference gradually reduces to zero. The findings demonstrate the necessity to incorporate charging impendence in station deployment in light of its significant effects on flow coverage and station locations. However, we caution that the degree of the effect may largely depend on the parameters in the charging impendence function. The values of these parameters should be carefully chosen based on empirical studies in the future.

Table 3. Comparison of range anxiety minimization model against the maximum flow model

B	Maximum flow model		Range anxiety minimization model		Different Station No.
	CFR	Location No.	CFR	Location No.	
1	**0.03**	**20**	**0.03**	**19**	**1**
2	0.06	17,19	0.06	17,19	0
3	0.12	17,18,19	0.12	17,18,19	0
4	0.14	10,14,20,21	0.14	10,14,20,21	0
5	0.20	10,14,20,21,22	0.20	10,14,20,21,22	0
6	0.25	14,20,21,22,23,24	0.25	14,20,21,22,23,24	0
7	0.32	10,14,20,21,22,23,24	0.32	10,14,20,21,22,23,24	0
8	0.36	8,10,14,20,21,22,23,24	0.36	8,10,14,20,21,22,23,24	0
9	**0.38**	**4,8,10,14,20,21,22,23,24**	**0.38**	**8,10,14,17,18,19,22,23,24**	**3**
10	0.43	10,14,17,18,19,20,21,22,23,24	0.43	10,14,17,18,19,20,21,22,23,24	0
11	0.47	8,10,14,17,18,19,20,21,22,23,24	0.47	8,10,14,17,18,19,20,21,22,23,24	0
12	0.50	4,8,10,14,17,18,19,20,21,22,23,24	0.50	4,8,10,14,17,18,19,20,21,22,23,24	0
13	0.52	4,8,10,13,14,17,18,19,20,21,22,23,24	0.52	4,8,10,13,14,17,18,19,20,21,22,23,24	0
14	0.55	8,10,11,12,13,14,17,18,19,20,21,22,23,24	0.55	8,10,11,12,13,14,17,18,19,20,21,22,23,24	0
15	**0.58**	**7,8,10,11,12,13,14,17,18,19,20,21,22,23,24**	**0.58**	**4,8,10,11,12,13,14,17,18,19,20,21,22,23,24**	**1**
16	0.60	4,7,8,10,11,12,13,14,17,18,19,20,21,22,23,24	0.60	4,7,8,10,11,12,13,14,17,18,19,20,21,22,23,24	0
17	0.63	3,4,7,8,10,11,12,13,14,17,18,19,20,21,22,23,24	0.63	3,4,7,8,10,11,12,13,14,17,18,19,20,21,22,23,24	0
18	0.65	1,2,4,5,8,10,11,12,13,14,17,18,19,20,21,22,23,24	0.65	1,2,4,5,8,10,11,12,13,14,17,18,19,20,21,22,23,24	0
19	0.67	1,2,3,4,5,8,10,11,12,13,14,17,18,19,20,21,22,23,24	0.67	1,2,3,4,5,8,10,11,12,13,14,17,18,19,20,21,22,23,24	0
20	0.69	1,2,3,4,5,7,8,10,11,12,13,14,17,18,19,20,21,22,23,24	0.69	1,2,3,4,5,7,8,10,11,12,13,14,17,18,19,20,21,22,23,24	0
21	**0.70**	**1,2,3,4,5,7,8,10,11,12,13,14,15,17,18,19,20,21,22,23,24**	**0.70**	**1,2,3,4,5,7,8,10,11,12,13,14,16,17,18,19,20,21,22,23,24**	**1**
22	0.72	1,2,3,4,5,7,8,10,11,12,13,14,15,16,17,18,19,20,21,22,23,24	0.72	1,2,3,4,5,7,8,10,11,12,13,14,15,16,17,18,19,20,21,22,23,24	0

23	**0.72**	**1,2,3,4,5,6,7,8,10,11,12,13,14,15,16,17,18,19,20,21,22,23,24**	**0.72**	**1,2,3,4,5,7,8,9,10,11,12,13,14,15,16,17,18,19,20,21,22,23,24**	**1**
24	0.72	1,2,3,4,5,6,7,8,9,10,11,12,13,14,15,16,17,18,19,20,21,22,23,24	0.72	1,2,3,4,5,6,7,8,9,10,11,12,13,14,15,16,17,18,19,20,21,22,23,24	0
25	0.73	1,2,3,4,5,6,7,8,9,10,11,12,13,14,15,16,17,18,19,20,21,22,23,24,25	0.73	1,2,3,4,5,6,7,8,9,10,11,12,13,14,15,16,17,18,19,20,21,22,23,24,25	0

Remark: instances with different station deployment are highlighted in bold.

Table 4. Comparison of the original model [DCSP] against the extended model [DCSPCI]

B	Original model [DCSP]		Extended model [DCSPCI]		Different Station No.
	CFR	Location No.	CFR	Location No.	
1	0.03	19	0.03	19	0
2	0.06	17,19	0.06	17,19	0
3	**0.12**	**17,18,19**	**0.08**	**14,17,19**	**1**
4	**0.15**	**13,17,18,19**	**0.12**	**14,17,19,22**	**2**
5	**0.2**	**10,14,20,21,22**	**0.14**	**13,14,17,19,22**	**3**
6	**0.25**	**14,20,21,22,23,24**	**0.17**	**8,10,14,17,19,22**	**4**
7	**0.32**	**10,14,20,21,22,23,24**	**0.19**	**8,10,13,14,17,19,22**	**4**
8	**0.36**	**8,10,14,20,21,22,23,24**	**0.21**	**4,8,10,13,14,17,19,22**	**4**
9	**0.4**	**8,9,10,14,20,21,22,23,24**	**0.23**	**3,4,8,10,13,14,17,19,22**	**5**
10	**0.43**	**10,14,17,18,19,20,21,22,23,24**	**0.25**	**1,2,4,5,8,10,14,17,19,22**	**5**
11	**0.47**	**8,10,14,17,18,19,20,21,22,23,24**	**0.28**	**1,2,4,5,8,10,13,14,17,19,22**	**5**
12	**0.51**	**8,9,10,14,17,18,19,20,21,22,23,24**	**0.30**	**1,2,3,4,5,8,10,13,14,17,19,22**	**6**
13	**0.53**	**8,9,10,13,14,17,18,19,20,21,22,23,24**	**0.31**	**1,2,4,5,8,10,13,14,17,19,22,23,24**	**4**
14	**0.56**	**8,10,11,12,13,14,17,18,19,20,21,22,23,24**	**0.33**	**1,2,3,4,5,8,10,13,14,17,19,22,23,24**	**5**
15	**0.6**	**8,9,10,11,12,13,14,17,18,19,20,21,22,23,24**	**0.34**	**1,2,3,4,5,8,10,11,13,14,17,19,22,23,24**	**5**
16	**0.63**	**7,8,9,10,11,12,13,14,17,18,19,20,21,22,23,24**	**0.36**	**1,2,3,4,5,8,10,11,12,13,14,17,19,22,23,24**	**5**
17	**0.65**	**1,4,5,8,10,11,12,13,14,17,18,19,20,21,22,23,24**	**0.37**	**1,2,3,4,5,7,8,10,11,12,13,14,17,19,22,23,24**	**3**
18	**0.68**	**1,2,4,5,8,10,11,12,13,14,17,18,19,20,21,22,23,24**	**0.38**	**1,2,3,4,5,7,8,10,11,12,13,14,16,17,19,22,23,24**	**3**

19	**0.71**	**1,2,3,4,5,8,10,11,12,13,14,17,18,19,20,21,22,23,24**	**0.39**	**1,2,3,4,5,7,8,10,11,12,13,14,17,19,20,21,22,23,24**	**1**
20	**0.73**	**1,2,3,4,5,7,8,10,11,12,13,14,17,18,19,20,21,22,23,24**	**0.40**	**1,2,3,4,5,7,8,10,11,12,13,14,16,17,19,20,21,22,23,24**	**1**
21	**0.74**	**1,2,3,4,5,7,8,10,11,12,13,14,15,17,18,19,20,21,22,23,24**	**0.40**	**1,2,3,4,5,7,8,9,10,11,12,13,14,16,17,19,20,21,22,23,24**	**2**
22	**0.75**	**1,2,3,4,5,7,8,10,11,12,13,14,15,16,17,18,19,20,21,22,23,24**	**0.41**	**1,2,3,4,5,6,7,8,9,10,11,12,13,14,16,17,19,20,21,22,23,24**	**2**
23	**0.75**	**1,2,3,4,5,7,8,9,10,11,12,13,14,15,16,17,18,19,20,21,22,23,24**	**0.41**	**1,2,3,4,5,6,7,8,9,10,11,12,13,14,15,16,17,19,20,21,22,23,24**	**1**
24	0.76	1,2,3,4,5,6,7,8,9,10,11,12,13,14,15,16,17,18,19,20,21,22,23,24	0.41	1,2,3,4,5,6,7,8,9,10,11,12,13,14,15,16,17,18,19,20,21,22,23,24	0
25	0.76	1,2,3,4,5,6,7,8,9,10,11,12,13,14,15,16,17,18,19,20,21,22,23,24,25	0.42	1,2,3,4,5,6,7,8,9,10,11,12,13,14,15,16,17,18,19,20,21,22,23,24,25	0

Remark: instances with different station deployment are highlighted in bold.

6.5 Sensitivity analyses

We proceed to analyze the impact of the vehicle parameter (i.e., the battery capacity), the user parameter (i.e., path deviation tolerance), and the system parameter (i.e., the budget) on the system performance. We will vary the concerned parameters in its feasible range while keeping the other parameters being the middle value in its feasible range introduced in Subsection 6.2. For example, for the sensitivity analysis of battery capacity, we will examine the results of DCSP under $E \in \{6,7,8,9,10\}$, $B = 13$, $\eta^w = 20\% L^w$ in the 25-node network. To facilitate the station deployment comparison under different parameter settings, the number of selected station locations in set $\{1,2,...,9\}$, $\{10,11,...,21\}$, and $\{22,...,25\}$, corresponding to the upper left corner (UL), the middle right hand (MR), and the lower bottom of the network (LB) respectively (see Figure 7), will be tabulated. We will also report the covered flow and uncovered flow volume and ratios (CF, UF, CFR, and UFR), the covered and uncovered OD pairs and ratios (CP, UP, CPR, and UPR), the accumulated range anxiety per covered EV driver (ARA), and the covered-flow-weighted average maximal driving range anxiety (MRA) calculated by $\sum_{w \in \bar{\mathcal{W}}} \left[f^w \max_j \{F(r_j^w)\} \right] / \sum_{w \in \bar{\mathcal{W}}} \left[f^w \right]$, where $\bar{\mathcal{W}}$ denotes the set of covered OD pairs.

Table 5 tabulates the results of the proposed model under different values of budget. The variations of CF&CP, ARA&MRA, and station locations are visualized in Figures 10-12 respectively. According to Figure 10, the covered flow volume rises steadily with the increase of budget, and the increment rate slows down when the budget exceeds 20. This can be explained by the fact that the proposed model covers as many flows as possible if budget permits. The covered number of OD pairs, by and large, follows a similar upward trend but with obvious fluctuation. For instance, the number of covered OD pairs declines from 70 to 60 as the budget increases from 9 to 11. As a matter of fact, more budget will offer the flexibility to the local authority to cover a smaller number of OD pairs associated with the largest flow volume. Another notable result as shown in Figure 11 is that both the ARA and MRA is not decreasing with more budget available, or broadly speaking, they increase with the rise of budget. This may again be attributed to the big-M component in the objective function of the proposed model, which places the flow coverage as the priority. The variations of MRA and ARA are similar, implying that the proposed model could also mitigate the worst-case range anxiety, although the primary goal is to reduce the accumulated range anxiety over a trip. As for the station deployment, Figure 12 shows that all EV charging stations are suggested to be established in the middle right hand of the network when the budget is quite limited (less than 4). As long as the budget exceeds 6, at least three stations should be built in the lower bottom of the network because we find that node 24 is a large travel demand attractor/generator in terms of its weight in the gravity model. When the budget goes beyond 14, the additional budget is directed to the station deployment at the upper left corner of the network until the budget exceeds 20.

Table 5. Effect of budget on the system performance in 25-node network

B	Station location			Flow coverage				OD pair coverage				ARA	MRA
	UL	MR	LB	CF	UF	CFR	UFR	CP	UP	CPR	UPR		
1	0	1	0	315	11,299	0.03	0.97	1	299	0.00	1.00	0.00	0.00
2	0	2	0	722	10,892	0.06	0.94	3	297	0.01	0.99	0.00	0.01
3	0	3	0	1,397	10,217	0.12	0.88	5	295	0.02	0.98	0.40	0.23
4	0	4	0	1,725	9,889	0.15	0.85	15	285	0.05	0.95	0.47	0.28
5	0	4	1	2,348	9,266	0.20	0.80	24	276	0.08	0.92	0.53	0.27
6	0	3	3	2,907	8,707	0.25	0.75	26	274	0.09	0.91	0.69	0.32
7	0	4	3	3,725	7,889	0.32	0.68	41	259	0.14	0.86	0.74	0.33
8	1	4	3	4,217	7,397	0.36	0.64	49	251	0.16	0.84	0.75	0.32
9	2	4	3	4,598	7,016	0.40	0.60	70	230	0.23	0.77	0.79	0.35
10	0	7	3	5,023	6,591	0.43	0.57	52	248	0.17	0.83	0.68	0.30
11	1	7	3	5,515	6,099	0.47	0.53	60	240	0.20	0.80	0.64	0.30
12	2	7	3	5,903	5,711	0.51	0.49	82	218	0.27	0.73	0.69	0.32
13	2	8	3	6,182	5,432	0.53	0.47	90	210	0.30	0.70	0.73	0.32
14	1	10	3	6,533	5,081	0.56	0.44	99	201	0.33	0.67	0.80	0.36
15	2	10	3	6,939	4,675	0.60	0.40	123	177	0.41	0.59	0.84	0.37
16	3	10	3	7,278	4,336	0.63	0.37	155	145	0.52	0.48	0.86	0.39
17	4	10	3	7,539	4,075	0.65	0.35	142	158	0.47	0.53	0.85	0.36
18	5	10	3	7,906	3,708	0.68	0.32	143	157	0.48	0.52	0.81	0.34
19	6	10	3	8,195	3,419	0.71	0.29	160	140	0.53	0.47	0.85	0.35
20	7	10	3	8,447	3,167	0.73	0.27	186	114	0.62	0.38	0.87	0.35
21	7	11	3	8,620	2,994	0.74	0.26	203	97	0.68	0.32	0.83	0.35
22	7	12	3	8,717	2,897	0.75	0.25	205	95	0.68	0.32	0.83	0.35
23	8	12	3	8,754	2,860	0.75	0.25	207	93	0.69	0.31	0.81	0.34
24	9	12	3	8,811	2,803	0.76	0.24	230	70	0.77	0.23	0.82	0.34
25	9	12	4	8,843	2,771	0.76	0.24	252	48	0.84	0.16	0.84	0.34

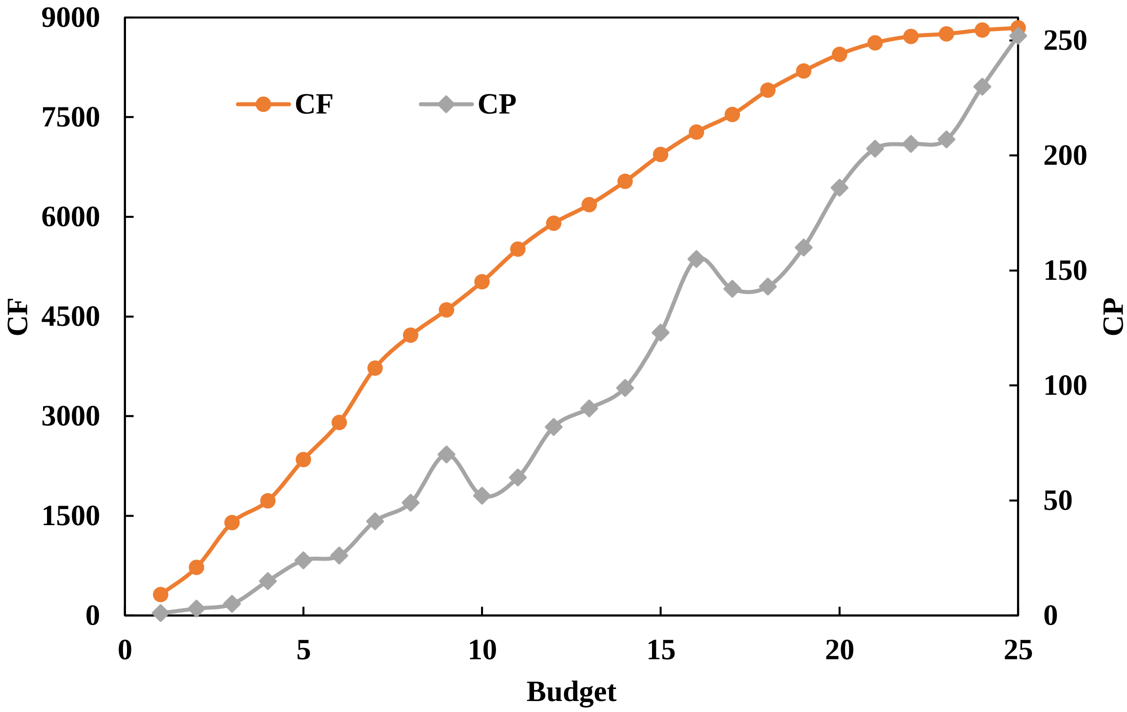

Figure 10. Variations of covered flow (CF) and covered OD pairs (CP) with the increase of budget

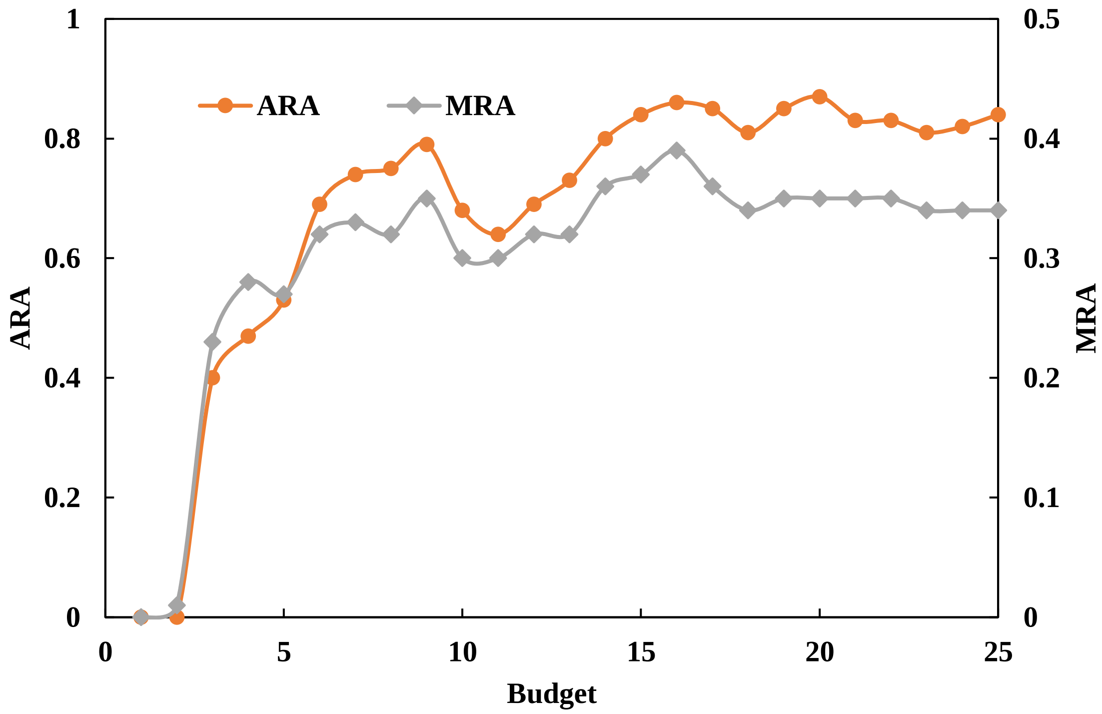

Figure 11. Variations of accumulated range anxiety (ARA) and maximal driving range anxiety (MRA) with the increase of budget

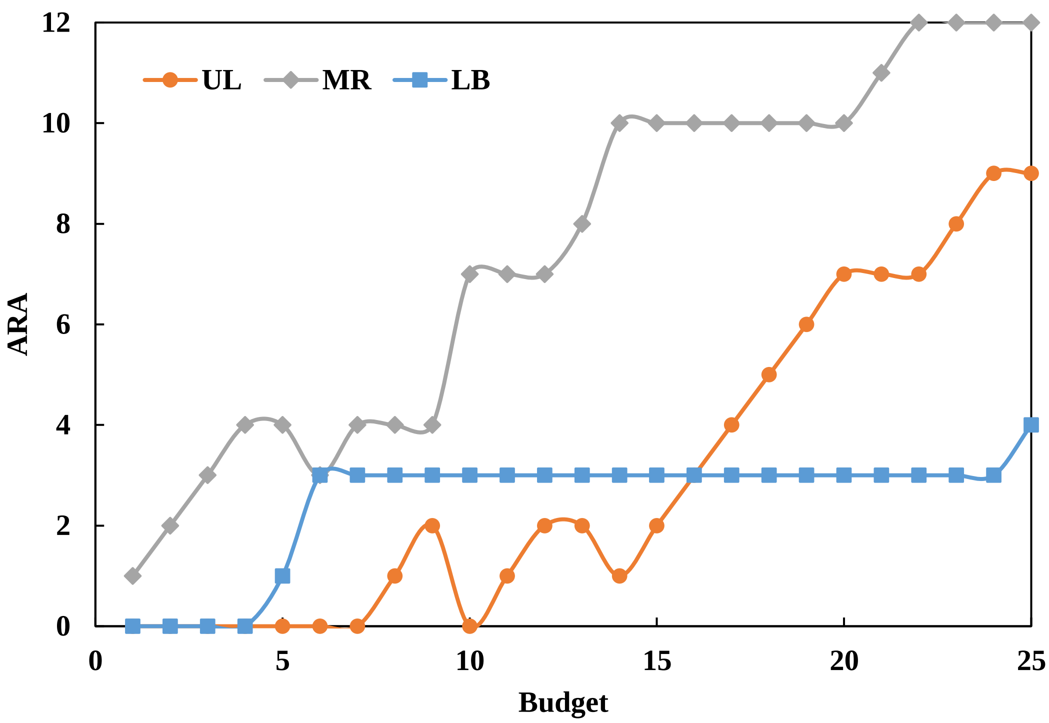

Figure 12. Variations of number of selected station locations in the upper left corner (UL), middle right hand (MR) and lower bottom (LB) of the network with the increase of budget

The results of the model under different values of battery capacity are summarized in Table 6. Figures 13-15 show how the variation of battery capacity affects the flow coverage, range anxiety of EV drivers and the station location, respectively. As can be seen, both the covered flow volume and OD pairs display an upward trend with the increase of battery capacity. The range anxiety-related parameters, i.e., ARA and MRA, are also affected by the battery capacity. The direction of influence, however, is somehow arbitrary. It is worthwhile to note that the accumulated range anxiety per covered EV driver is almost doubled although the battery capacity only grows from 6 to 7, and it returns to around 0.34 when the battery capacity is increased to be 8 or larger. By comparing the values of ARA and MRA under battery capacity of 6, 8, and 10, we can find that the increase of battery capacity could eliminate the extreme case of range anxiety even if the accumulated range anxiety is not sensitive to it. Regarding the station location, there would be a station located in the lower bottom of the network in all instances, while some of the rest stations will be deployed in the upper left corner or the middle right hand of the network subject to fluctuation.

Table 6. Effect of battery capacity on the system performance in 25-node network

E	Station location	Flow coverage	OD pair coverage	ARA	MRA

	UL	MR	LB	CF	UF	CFR	UFR	CP	UP	CPR	UPR		
6	4	8	1	3,276	8,338	0.28	0.72	28	272	0.09	0.91	0.34	0.33
7	4	8	1	5,515	6,099	0.47	0.53	77	223	0.26	0.74	0.64	0.38
8	2	10	1	6,182	5,432	0.53	0.47	90	210	0.30	0.70	0.34	0.25
9	3	9	1	7,793	3,821	0.67	0.33	97	203	0.32	0.68	0.38	0.25
10	4	8	1	8,489	3,125	0.73	0.27	116	184	0.39	0.61	0.34	0.22

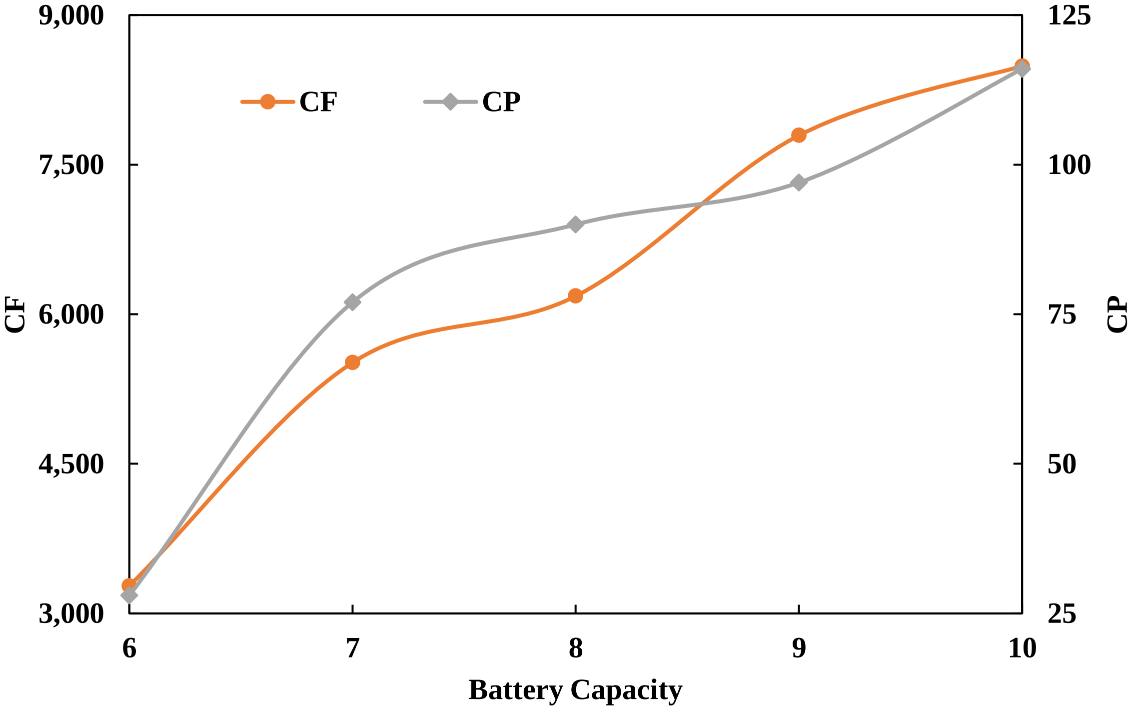

Figure 13. Variations of covered flow (CF) and covered OD pairs (CP) with the increase of battery capacity

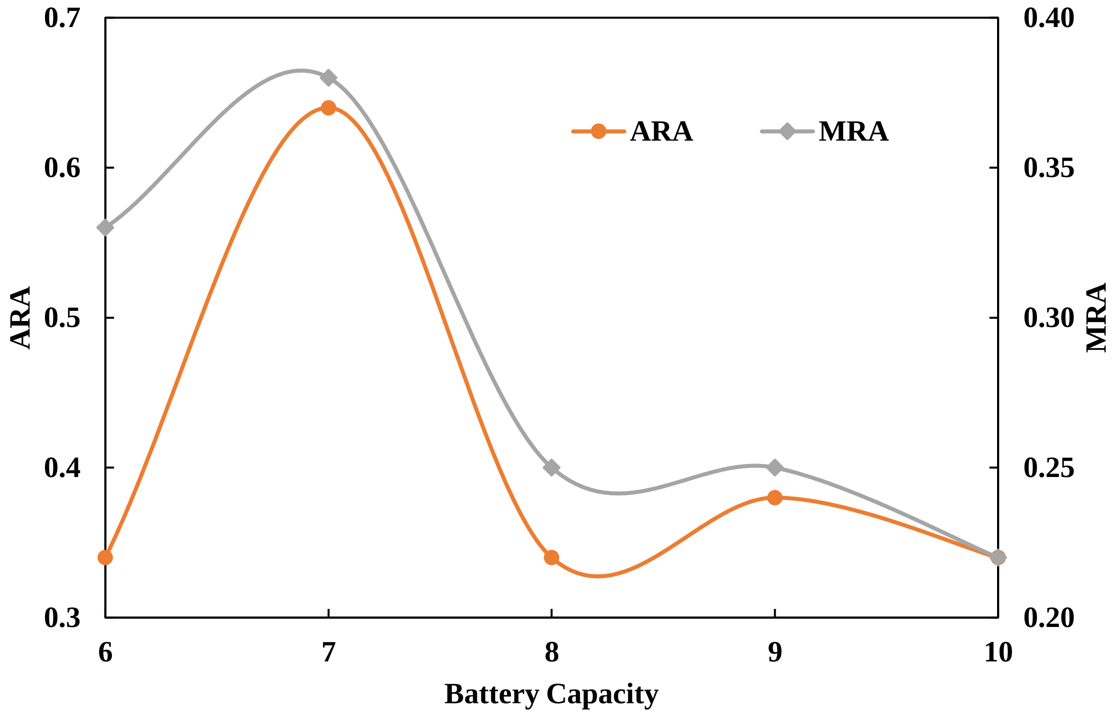

Figure 14. Variations of accumulated range anxiety (ARA) and maximal driving range anxiety (MRA) with the increase of battery capacity

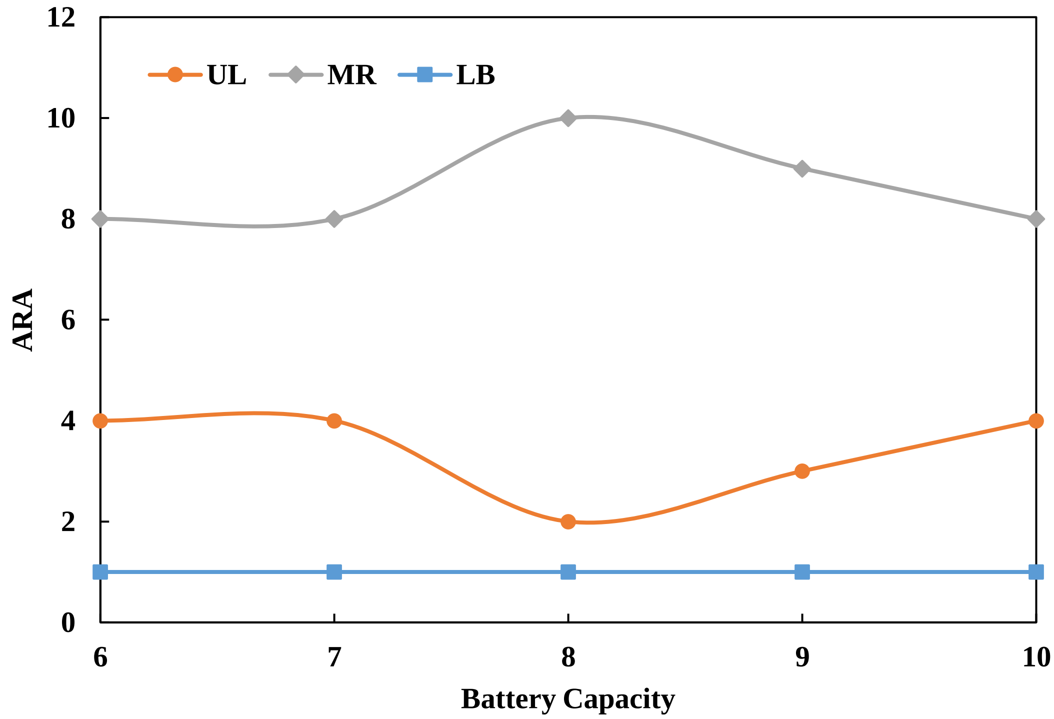

Figure 15. Variations of number of selected station locations in the upper left corner (UL), middle right hand (MR) and lower bottom (LB) of the network with the increase of battery capacity

The impact of path deviation tolerance on system performance is illustrated in Figures 16-18. The relevant data are tabulated in Table 7. It shows the positive influence of path deviation on the flow and OD pair coverage. The effect, however, exhibits a nonlinear and piece-wise pattern. For example, the covered flow remains steady around 6100 under a path deviation tolerance smaller than 0.3 but swiftly increases to about 6600 when the tolerance is 0.4. It seems that the station deployment is insensitive to the path deviation tolerance unless the path deviation tolerance exceeds 0.3. Analogous to the budget, the increase of path deviation tolerance results in more flows to be covered but both the accumulated and maximal range anxiety per covered EV driver negatively increase simultaneously.

Table 7. Effect of path deviation tolerance on the system performance in 25-node network

η	Station location			Flow coverage				OD pair coverage				ARA	MRA
	UL	MR	LB	CF	UF	CFR	UFR	CP	UP	CPR	UPR		
0	2	10	1	6025	5,589	0.52	0.48	80	220	0.27	0.73	0.59	0.29
0.1	2	10	1	6,121	5,493	0.53	0.47	82	218	0.27	0.73	0.70	0.30
0.2	2	10	1	6,182	5,432	0.53	0.47	90	210	0.30	0.70	0.69	0.32
0.3	2	10	1	6,202	5,412	0.53	0.47	91	209	0.30	0.70	0.73	0.33
0.4	0	12	1	6,610	5,004	0.57	0.43	102	198	0.34	0.66	0.90	0.41
0.5	0	12	1	6,731	4,883	0.58	0.42	106	194	0.35	0.65	0.94	0.42

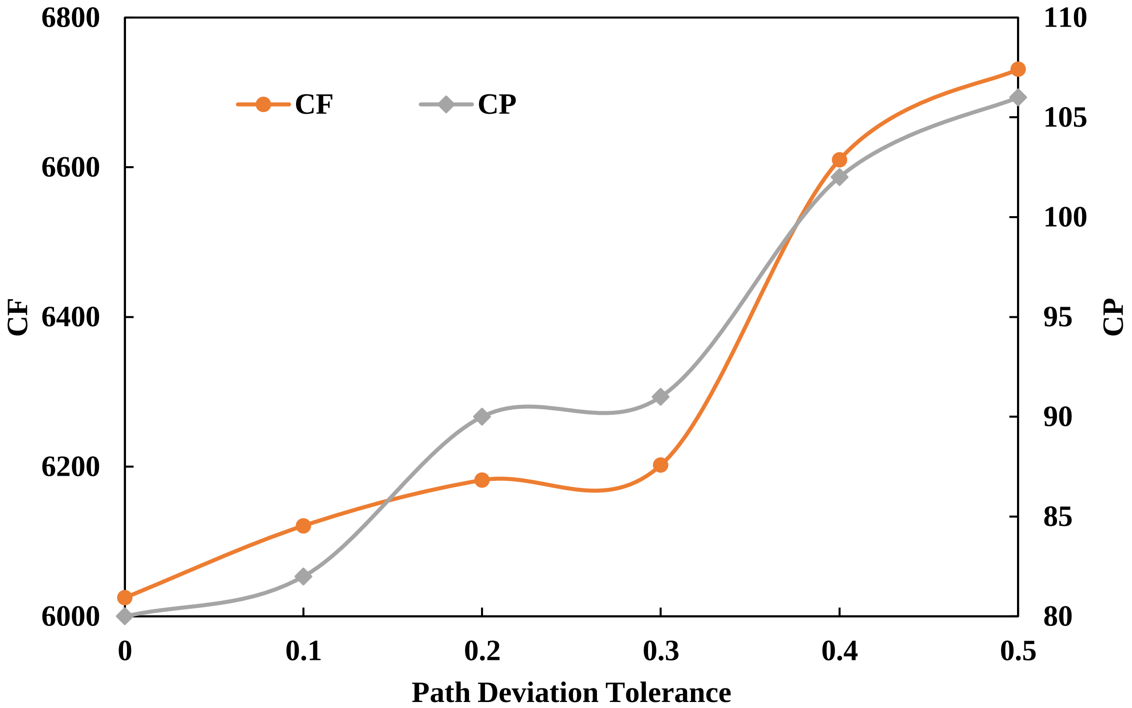

Figure 16. Variations of accumulated range anxiety (ARA) and maximal driving range anxiety (MRA) with the increase of path deviation tolerance

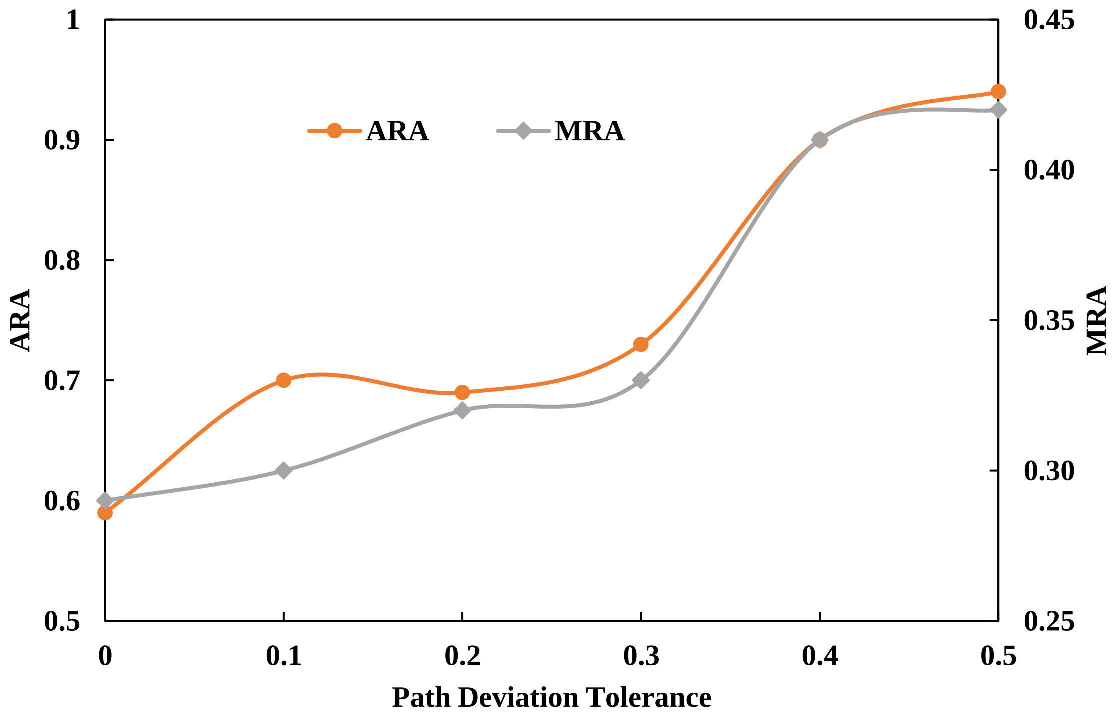

Figure 17. Variations of accumulated range anxiety (ARA) and maximal driving range anxiety (MRA) with the increase of path deviation tolerance

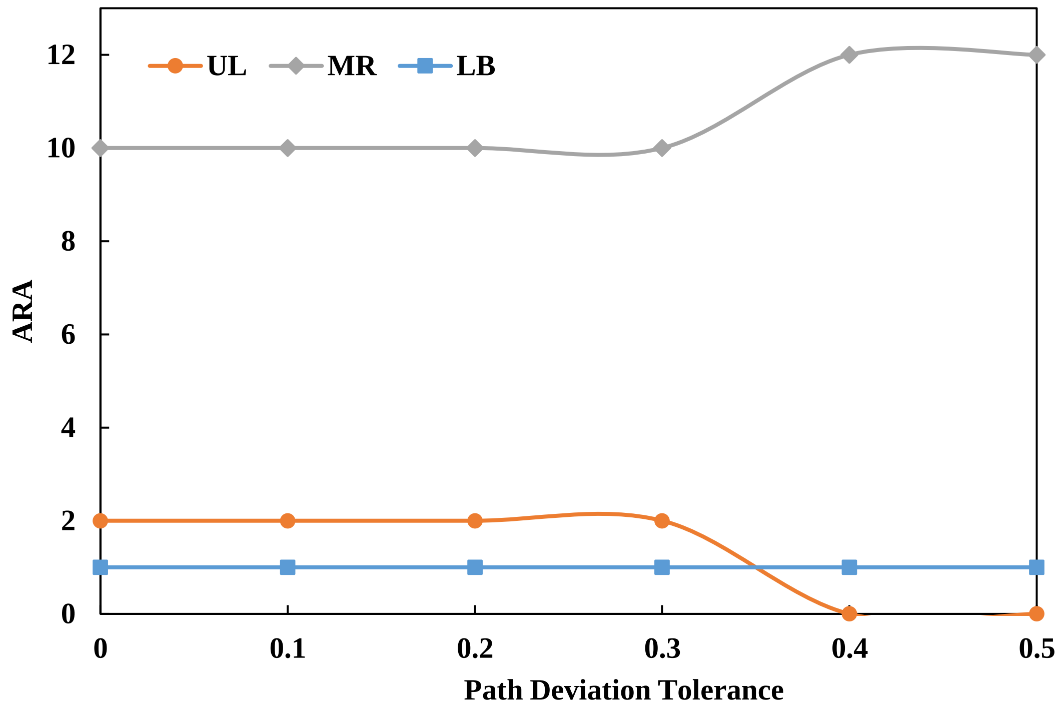

Figure 18. Variations of number of selected station locations in the upper left corner (UL), middle right hand (MR) and lower bottom (LB) of the network with the increase of path deviation tolerance

6.6 Location comparison under different subsets of OD pairs

One important parameter that is believed to largely affect the computational performance of the proposed models is the number of OD pairs. In real networks, the sum of flows over a small number of OD pairs generally accounts for a larger portion of the total flows over all OD pairs. Therefore, it is insightful and practically significant to compare the optimal locations under different subsets of OD pairs to explore whether the optimal locations obtained by considering only a subset of OD pairs with the largest flow volume are also “good” locations for the charging stations that minimize the total range anxiety of travelers when all OD pairs are considered. As such, we sort the 435 OD pairs of Texas highway network in descending order in terms of flow volume and pick up the top 100, 150, 200, …, 400, and 435 OD pairs respectively. A total of 8 instances with an increasing number of OD pairs and accordingly an increasing volume of traffic flows are created under the same parameter setting, i.e., $B \in \{10, 30, 50\}$, $E = 40$, and $\eta^w = 5\% L^w$. We report the flow ratio (FR) of each subset of OD pairs to the total flow volume of all OD pairs in Table 8. For ease of comparison, the number of same locations (SLN) suggested by the model under each subset of OD pairs and all OD pairs as well as the correspondent ratio to the total number of locations to be chosen(SLR), i.e., the budget, are tabulated. It shows that in Texas highway network, the sum of flows of the top 100 OD pairs accounts for over 90% of the total flow volume. Under the budget of 10, 8 out of 10 locations are the same with the locations obtained by considering all OD pairs and the overlap ratio (i.e., SLN) is 80%, demonstrating the credibility of considering only a subset of OD pairs in the determination of station deployment. This, however, may not be true for instances under large budget values. The SLR drops down to 58% when the budget increases to 50. This phenomenon also occurs in instances with a larger subset of OD pairs. In fact, the average overlap ratio over the instances with different subsets OD pairs under budget 10 is obviously larger than that under the budget of 30 or 50. Despite the decreasing credibility of the suggested locations with the increase of budget, the average SLR is no less than 0.74, meaning that averagely 74% of the locations obtained by considering only a subset of OD pairs is still optimal for instances with all OD pairs considered. Under a specific budget, different subsets of OD pairs are often associated with different SLR. For example, under the budget of 10, considering the top 200 OD pairs can produce exactly the same optimal locations to the results considering all OD pairs, whereas the SLR is only 70% if only the top 100 OD pairs are considered. On average, considering the top 250 OD pairs produces the highest overlap ratio and most reliable locations.

Table 8. Location comparison under different subsets of OD pairs

OD No.	FR	B=10		B=30		B=50		Average SLR over budget
		SLN	SLR	SLN	SLR	SLN	SLR	
100	0.908	8	0.80	23	0.77	29	0.58	0.72
150	0.942	7	0.70	22	0.73	36	0.72	0.72
200	0.963	10	1.00	21	0.70	38	0.76	0.82
250	0.977	10	1.00	23	0.77	39	0.78	0.85
300	0.986	9	0.90	19	0.63	36	0.72	0.75
350	0.993	9	0.90	23	0.77	37	0.74	0.80
400	0.998	8	0.80	24	0.80	38	0.76	0.79
Average SLR over OD pair			0.87		0.74		0.75	

7. Conclusions and Future Research

This study investigates the optimal deployment of EV charging stations considering drivers' range anxiety and path deviation. EV drivers feel uncomfortable when the SOC of battery declines below a threshold caused by the fear of being stranded in the middle of a trip. The range anxiety profile is assumed to be a nonlinear function based on the empirical studies in the literature. The drivers may also take a deviation path other than the shortest path between the OD pair for refueling. In order to minimize the accumulated range anxiety of concerned travelers over the entire trips, we developed for the first time a compact model with a polynomial number of constraints by explicitly formulating the charging logic and path detour behavior in the model. The compact model favorably circumvents the computationally extensive path and combination pre-generation required by traditional FRLM/DFRLM. The consideration of nonlinear range anxiety function makes the model was not readily solvable by commercial solvers. After demonstrating the convexity of the model, an efficient outer-approximation method was proposed to obtain an ε-optimal solution to the underlying problem. The model was further extended to incorporate the charging impedance, e.g., the charging time and cost. A 25-node benchmark network and a real-life Texas highway network were used in the numerical experiments to evaluate the efficiency of the proposed model and algorithm, and to examine the impact of the battery capacity, path deviation tolerance, budget and the subset of OD pairs on the optimal solution and the performance of the system.

Further research work can be undertaken in several aspects. First, the proposed solution method is not computationally efficient for large networks. It is thus important to improve the efficiency of current algorithm or develop new and customized solution methods for implementation in large-scale problems in the future. Second, more studies are necessary to quantitatively analyze the range anxiety and travel behavior of EV drivers, and more importantly, analytically calibrate the range anxiety profile and the charging impedance function from reliable data. Third, the compact model can be used as a benchmark model to be extended from several aspects, such as the incorporation of parameter uncertainty in charging demand, driving range, electricity consumption, as well as the consideration of flow-dependent travel time or traffic congestion effect, the station capacity, the partial charging, and the queuing behavior at stations, etc. Last but not the least, the long period of station construction and the variation of optimal station location under different values of budget and battery capacity calls for the development of a dedicated approach for the multi-period planning for the station deployment.

Acknowledgements

We are grateful to Professor Chungmok Lee and Professor Jinil Han for providing us with the detailed data of Texas highway network. This study is supported by the Hong Kong Polytechnic University (1-BE1V).

Appendix. Notations

Indices and sets

$\mathcal{N}$	Set of nodes
$\mathcal{A}$	Set of links
$\mathcal{W}$	Set of OD pairs
$\mathcal{S}$	Set of destinations
$\mathcal{I}$	Set of candidate locations for EV charging stations
i, j	Indices for node
(i, j)	Index for link
$r(w)$	Index for origin node of an OD pair $w \in \mathcal{W}$
$s(w)$	Index for destination node of an OD pair $w \in \mathcal{W}$

Known parameters or functions

l_{ij}	Length of link (i, j)
d_{ij}	Electricity consumption of link (i, j)
f^w	Flow volume of an OD pair $w \in \mathcal{W}$
c_i	Construction cost of an EV charging station at node $i \in \mathcal{I}$
B	Total budget for EV charging station construction
E	Usable battery capacity of an EV per a full battery charge
E_O	SOC threshold at departure
E_D	SOC threshold at arrival
L^w	Length of the shortest path for an OD pair w
η^w	Pre-specified tolerance for detour distance of OD pair w
$R_{\max}$	Maximal range anxiety of an EV driver experienced at the minimal SOC
E_{comf}	Comfortable range threshold above which EV drivers are free from range anxiety
$S(t)$	SOC profile during battery discharging as a function of travel time
$R(t)$	Range anxiety profile during battery discharging/traveling as a function of travel time
$\bar{R}(r)$	Accumulated range anxiety along a path segment as a function of final SOC at the end node of the path segment
$S^{-1}(\bullet)$	Inverse function of SOC profile $S(\bullet)$
α_i	Average charging impedance incurred at station i that is independent of the charging amount
β_i	Charging-amount-dependent impedance incurred at station i per unit amount of charging

Decision variables

y_i	Binary variable indicating if a station should be built at location i
x_{ij}^w	Binary variable indicating if the flow of OD pair w will traverse link (i, j)
e_i^w	The remaining electricity in battery rightly after traversing node i

r_j^w SOC upon the EVs of OD pair w arriving an EV charging station j or the destination $s(w)$

y_i^w Binary variable indicating if the travelers of OD pair w will charge at the station i

References

Anderson, E.W., Sullivan, M.W., 1993. The antecedents and consequences of customer satisfaction for firms. *Marketing Science* 12(2), 125-143.

Arslan, O., Karaşan, O.E., 2016. A Benders decomposition approach for the charging station location problem with plug-in hybrid electric vehicles. *Transportation Research Part B: Methodological* 93, 670-695.

Bunsen, T., Cazzola, P., Gorner, M., Paoli, L., Scheffer, S., Schuitmaker, R., Tattini, J., Teter, J., 2018. Global EV Outlook 2018: Towards cross-modal electrification. http://www.oecd.org/publications/global-ev-outlook-2018-9789264302365-en.htm (accessed 15.08.2019).

Capar, I., Kuby, M., Leon, V.J., Tsai, Y.-J., 2013. An arc cover–path-cover formulation and strategic analysis of alternative-fuel station locations. *European Journal of Operational Research* 227(1), 142-151.

Chittenden County RPC (CCR), 2014. Electric Vehicle Charging Station Guidebook Planning for Installation and Operation. http://www.driveelectricvt.com/Media/Default/docs/electric-vehicle-charging-station-guidebook.pdf (accessed 15.08.2019).

Chen, L.-H., Chen, C.-N., 2014. A QFD-based mathematical model for new product development considering the target market segment. *Journal of Applied Mathematics 2014,* Article ID 594150, 1-10.

Chen, Z., He, F., Yin, Y., 2016. Optimal deployment of charging lanes for electric vehicles in transportation networks. *Transportation Research Part B: Methodological* 91, 344-365.

Chung, S.H., Kwon, C., 2015. Multi-period planning for electric car charging station locations: A case of Korean Expressways. *European Journal of Operational Research* 242(2), 677-687.

Dong, J., Liu, C., Lin, Z., 2014. Charging infrastructure planning for promoting battery electric vehicles: An activity-based approach using multiday travel data. *Transportation Research Part C: Emerging Technologies* 38, 44-55.

Duran, M.A., Grossmann, I.E., 1986. An outer-approximation algorithm for a class of mixed-integer nonlinear programs. *Mathematical Programming* 36(3), 307-339.

Egbue, O., Long, S., 2012. Barriers to widespread adoption of electric vehicles: An analysis of consumer attitudes and perceptions. *Energy Policy* 48, 717-729.

Franke, T., Neumann, I., Bühler, F., Cocron, P., Krems, J.F., 2012. Experiencing range in an electric vehicle: Understanding psychological barriers. *Applied Psychology* 61(3), 368-391.

Ghamami, M., Zockaie, A., Nie, Y.M., 2016. A general corridor model for designing plug-in electric vehicle charging infrastructure to support intercity travel. *Transportation Research Part C: Emerging Technologies* 68, 389-402.

Graham-Rowe, E., Gardner, B., Abraham, C., Skippon, S., Dittmar, H., Hutchins, R., Stannard, J., 2012. Mainstream consumers driving plug-in battery-electric and plug-in hybrid electric cars: A qualitative analysis of responses and evaluations. *Transportation Research Part A: Policy and Practice* 46(1), 140-153.

Grigoroudis, E., Siskos, Y., 2009. *Customer satisfaction evaluation: Methods for measuring and implementing service quality*. Springer Science & Business Media.

Grossmann, I.E., Kravanja, Z., 1995. Mixed-integer nonlinear programming techniques for process systems engineering. *Computers & Chemical Engineering* 19, 189-204.

Guo, F., Yang, J., Lu, J., 2018. The battery charging station location problem: Impact of users' range anxiety and distance convenience. *Transportation Research Part E: Logistics and Transportation Review* 114, 1-18.

He, F., Wu, D., Yin, Y., Guan, Y., 2013. Optimal deployment of public charging stations for plug-in hybrid electric vehicles. *Transportation Research Part B: Methodological* 47, 87-101.

He, F., Yin, Y., Zhou, J., 2015. Deploying public charging stations for electric vehicles on urban road networks. *Transportation Research Part C: Emerging Technologies* 60, 227-240.

He, J., Yang, H., Tang, T. Q., Huang, H. J., 2018. An optimal charging station location model with the consideration of electric vehicle's driving range. *Transportation Research Part C: Emerging Technologies, 86*, 641-654.

He, J., Yang, H., Tang, T. Q., Huang, H. J., 2020. Optimal deployment of wireless charging lanes considering their adverse effect on road capacity. *Transportation Research Part C: Emerging Technologies, 111*, 171-184.

Hodgson, M.J., 1990. A flow-capturing location-allocation model. *Geographical Analysis* 22(3), 270-279.

Huang, Y., Li, S., Qian, Z.S., 2015. Optimal deployment of alternative fueling stations on transportation networks considering deviation paths. *Networks and Spatial Economics* 15(1), 183-204.

Kim, J.-G., Kuby, M., 2012. The deviation-flow refueling location model for optimizing a network of refueling stations. *International Journal of Hydrogen Energy* 37(6), 5406-5420.

Kuby, M., Lim, S., 2005. The flow-refueling location problem for alternative-fuel vehicles. *Socio-Economic Planning Sciences* 39(2), 125-145.

Kuby, M., Lim, S., 2007. Location of alternative-fuel stations using the flow-refueling location model and dispersion of candidate sites on arcs. *Networks and Spatial Economics* 7(2), 129-152.

Lee, C., Han, J., 2017. Benders-and-Price approach for electric vehicle charging station location problem under probabilistic travel range. *Transportation Research Part B: Methodological* 106, 130-152.

Li, S., Huang, Y., Mason, S.J., 2016. A multi-period optimization model for the deployment of public electric vehicle charging stations on network. *Transportation Research Part C: Emerging Technologies* 65, 128-143.

Liu, H., Wang, D.Z., 2017. Locating multiple types of charging facilities for battery electric vehicles. *Transportation Research Part B: Methodological* 103, 30-55.

Mak, H.-Y., Rong, Y., Shen, Z.-J.M., 2013. Infrastructure planning for electric vehicles with battery swapping. *Management Science* 59(7), 1557-1575.

MirHassani, S., Ebrazi, R., 2012. A flexible reformulation of the refueling station location problem. *Transportation Science* 47(4), 617-628.

Morrow, K., Darner, D., Francfort, J., 2008. US Department of Energy Vehicle Technologies Program--Advanced Vehicle Testing Activity--Plug-in Hybrid Electric Vehicle Charging Infrastructure Review. Idaho National Laboratory (INL).

Neubauer, J., Wood, E., 2014. The impact of range anxiety and home, workplace, and public charging infrastructure on simulated battery electric vehicle lifetime utility. *Journal of Power Sources* 257, 12-20.

Nie, Y.M., Ghamami, M., 2013. A corridor-centric approach to planning electric vehicle charging infrastructure. *Transportation Research Part B: Methodological* 57, 172-190.

Nilsson, M., 2011. Electric vehicles: The phenomenon of range anxiety. *Report for the ELVIRE Project*. http://e-mobility-nsr.eu/fileadmin/user_upload/downloads/info-pool/the_phenomenon_of_range_anxiety_elvire.pdf (accessed 15.08.2019).

Nissan, 2019. Nissan LEAF EV. https://www.nissanusa.com/vehicles/electric-cars/leaf.html (accessed 15.08.2019).

Pelletier, S., Jabali, O., Laporte, G., Veneroni, M., 2017. Battery degradation and behaviour for electric vehicles: Review and numerical analyses of several models. *Transportation Research Part B: Methodological* 103, 158-187.

Rauh, N., Franke, T., Krems, J.F., 2015. Understanding the impact of electric vehicle driving experience on range anxiety. *Human Factors* 57(1), 177-187.

Sathaye, N., Kelley, S., 2013. An approach for the optimal planning of electric vehicle infrastructure for highway corridors. *Transportation Research Part E: Logistics and Transportation Review* 59, 15-33.

Sierzchula, W., Bakker, S., Maat, K., Van Wee, B., 2014. The influence of financial incentives and other socio-economic factors on electric vehicle adoption. *Energy Policy* 68, 183-194.

Smith, M., Castellano, J., 2015. Costs associated with non-residential electric vehicle supply equipment: Factors to consider in the implementation of electric vehicle charging stations. Technical Report DOE/EE-1289, US Department of Energy.

Valentine-Urbschat, M., Bernhart, W., 2009. Powertrain 2020–the future drives electric. *Roland Berger Strategy Consultants* 9.

Varvarezos, D.K., Grossmann, I.E., Biegler, L.T., 1992. An outer-approximation method for multiperiod design optimization. *Industrial & Engineering Chemistry Research* 31(6), 1466-1477.

Wang, C., He, F., Lin, X., Shen, Z. J. M., Li, M., 2019. Designing locations and capacities for charging stations to support intercity travel of electric vehicles: An expanded network approach. *Transportation Research Part C: Emerging Technologies*, *102*, 210-232.

Wang, S., Meng, Q., 2012. Sailing speed optimization for container ships in a liner shipping network. *Transportation Research Part E: Logistics and Transportation Review* 48(3), 701-714.

Wang, Y.-W., Lin, C.-C., 2009. Locating road-vehicle refueling stations. *Transportation Research Part E: Logistics and Transportation Review* 45(5), 821-829.

Wang, Y.-W., Wang, C.-R., 2010. Locating passenger vehicle refueling stations. *Transportation Research Part E: Logistics and Transportation Review* 46(5), 791-801.

Wang, Y., Meng, Q., Du, Y., 2015. Liner container seasonal shipping revenue management. *Transportation Research Part B: Methodological* 82, 141-161.

Xu, M., Meng, Q., 2019. Fleet sizing for one-way electric carsharing services considering dynamic vehicle relocation and nonlinear charging profile. *Transportation Research Part B: Methodological* 128, 23-49.

Xu, M., Meng, Q., Liu, K., 2017a. Network user equilibrium problems for the mixed battery electric vehicles and gasoline vehicles subject to battery swapping stations and road grade constraints. *Transportation Research Part B: Methodological* 99, 138-166.

Xu, M., Meng, Q., Liu, K., Yamamoto, T., 2017b. Joint charging mode and location choice model for battery electric vehicle users. *Transportation Research Part B: Methodological* 103, 68-86.

Xu, M., Meng, Q., Liu, Y., 2017c. Public's perception of adopting electric vehicles: a case study of Singapore. *Journal of the Eastern Asia Society for Transportation Studies* 12, 285-298.

Xu, M., Meng, Q., Liu, Z., 2018. Electric vehicle fleet size and trip pricing for one-way carsharing services considering vehicle relocation and personnel assignment. *Transportation Research Part B: Methodological* 111, 60-82.

Yang, J., Guo, F., Zhang, M., 2017. Optimal planning of swapping/charging station network with customer satisfaction. *Transportation Research Part E: Logistics and Transportation Review* 103, 174-197.

Yang, Y., Yao, E., Yang, Z., Zhang, R., 2016. Modeling the charging and route choice behavior of BEV drivers. *Transportation Research Part C: Emerging Technologies* 65, 190-204.

Yıldız, B., Arslan, O., Karaşan, O.E., 2016. A branch and price approach for routing and refueling station location model. *European Journal of Operational Research* 248(3), 815-826.

Yıldız, B., Olcaytu, E., Şen, A., 2019. The urban recharging infrastructure design problem with stochastic demands and capacitated charging stations. *Transportation Research Part B: Methodological* 119, 22-44.

Yuan, Q., Hao, W., Su, H., Bing, G., Gui, X., Safikhani, A., 2018. Investigation on range anxiety and safety buffer of battery electric vehicle drivers. *Journal of Advanced Transportation* 2018, Article ID 8301209, 1-11.

Zhang, A., Kang, J. E., Kwon, C., 2020. Multi-day scenario analysis for battery electric vehicle feasibility assessment and charging infrastructure planning. *Transportation Research Part C: Emerging Technologies*, *111*, 439-457.